D.B., and D.Y.G. provided reagents and conceptual advice; M.K.E., S.E.C., and K.E. wrote the initial draft of the manuscript; and all authors provided critical review and final approval of the manuscript. All relevant data are within this paper and the supplementary materials. Enteroids are available via a materials transfer agreement from Baylor College of Medicine. Baylor College of Medicine has filed a patent application related to this work: Cultivation of human noroviruses; provisional patent application no. 62/236,294.

SUPPLEMENTARY MATERIALS
www.sciencemag.org/content/353/6306/1387/suppl/DC1
Materials and Methods
Figs. S1 to S11
Table S1
References (*41*–*47*)

25 February 2016; accepted 18 August 2016
Published online 25 August 2016
10.1126/science.aaf5211

NEUROSCIENCE

The TRPM2 channel is a hypothalamic heat sensor that limits fever and can drive hypothermia

Kun Song,[1]*† Hong Wang,[1]† Gretel B. Kamm,[1]† Jörg Pohle,[1] Fernanda de Castro Reis,[2] Paul Heppenstall,[2,3] Hagen Wende,[1] Jan Siemens[1,3]‡

Body temperature homeostasis is critical for survival and requires precise regulation by the nervous system. The hypothalamus serves as the principal thermostat that detects and regulates internal temperature. We demonstrate that the ion channel TRPM2 [of the transient receptor potential (TRP) channel family] is a temperature sensor in a subpopulation of hypothalamic neurons. TRPM2 limits the fever response and may detect increased temperatures to prevent overheating. Furthermore, chemogenetic activation and inhibition of hypothalamic TRPM2-expressing neurons in vivo decreased and increased body temperature, respectively. Such manipulation may allow analysis of the beneficial effects of altered body temperature on diverse disease states. Identification of a functional role for TRP channels in monitoring internal body temperature should promote further analysis of molecular mechanisms governing thermoregulation and foster the genetic dissection of hypothalamic circuits involved with temperature homeostasis.

Core body temperature (T_{core}) is normally maintained very accurately in mammals within a narrow range around 37°C and serves as an important vital sign that is routinely monitored in hospitalized patients. Pathological conditions such as infections and systemic inflammation cause fever (*1*, *2*), an increase in the body's temperature that is thought to be mediated by prostaglandin E_2 (PGE_2)–induced inhibition of warm-sensitive neurons (WSNs) in the hypothalamic thermoregulatory center (*3*). Adverse drug-induced fluctuations in T_{core} can have severe and even fatal consequences (*4*). Conversely, clinically controlled modulation of T_{core} has beneficial effects and can prevent tissue damage, promote trauma recovery (*5*, *6*), or help decrease obesity (*7*).

The preoptic area (POA) of the hypothalamus serves as a thermostat, integrating temperature information to orchestrate the autonomous and behavioral adaptations needed to achieve thermal homeostasis (*3*, *8*). POA neurons receive and integrate information from peripheral temperature sensors located in the skin, spinal cord, and viscera. Local POA warming and cooling experiments (*9*–*13*) and genetic manipulations (*14*) have shown that this region of the central nervous system also detects local brain temperature changes, which have a strong impact on T_{core}. In fact, temperature changes in the POA can exert a dominant effect on T_{core} and can override lower-priority temperature inputs from peripheral temperature sensors, such as those located in the skin (*15*, *16*). Warming of the POA induces heat dissipation mechanisms such as cutaneous vasodilation, evaporative heat loss mechanisms, and behavioral adaptations, whereas cooling of the POA triggers heat conservation and thermogenesis.

POA neurons exhibiting pronounced temperature sensitivity have been described in in vivo models and in vitro preparations (*17*–*19*). WSNs enhance their firing rate upon warming, a process that is thought to relay temperature information to peripheral organs to promote heat loss (*3*). Conversely, a drop in deep brain temperature inhibits WSNs, a process that correlates with induction of thermogenesis and heat gain.

However, the genetic identity of WSNs and the molecular basis of their temperature sensitivity have remained elusive. Our work defined a population of WSNs that controls temperature homeostasis and identified a transient receptor potential (TRP) ion channel that subserves thermodetection in hypothalamic neurons.

TRPM2 is a heat sensor in a subset of POA neurons

To identify thermosensory molecules in the thermoregulatory center of the hypothalamus, we established calcium imaging as a means to monitor warming-induced responses of primary POA neuronal cultures (fig. S1, A to F). We applied a stringent criterion to identify WSNs by fura-2–mediated calcium imaging. We only counted neurons as WSNs if their relative increase in signal on receiving a thermal stimulus (up to 45°C) was larger than the mean fura-2 signal plus 5 times the standard deviation (5SD) of thermally unresponsive human embryonic kidney–293 cells subjected to the same temperature stimulus (fig. S1, E and F). This procedure allowed us to account and correct for the small unspecific temperature effect on the fluorescent fura-2 signal (*20*) (see fig. S1F and table S1 for details). We found that 16.3 ± 4.7% (mean ± SEM; n = 6 mice) of cultured POA neurons responded to warming, a fraction that is in the same range (10 to 16%) observed in electrophysiological studies of rodent POA cultures (*21*, *22*) and slightly lower than WSN percentages (20 to 40%) observed in POA slice preparations (*17*, *23*). Extracellular calcium appeared to be the source of the temperature-triggered increase in intracellular concentrations of free calcium, because chelation of external calcium abolished the response, whereas depletion of intracellular calcium stores did not have any effect on warm sensitivity (fig. S1, D and G).

Several ion channels are thermosensitive, exemplified by a steep temperature dependence (Q_{10} coefficient) of their opening probabilities. In particular, cationic TRP ion channels have been identified as thermosensors in the peripheral nervous system and function in the detection of ambient temperature changes (*24*–*27*).

To identify candidate channels mediating the observed warm sensitivity in neuronal POA cultures, we tested various inhibitors and agonists of TRPs and other thermosensitive ion channels (fig. S1, H to L). The calcium response appeared to be mediated by direct Ca^{2+} flux through a thermosensitive ion channel and not an indirect readout of voltage-gated channels, because nifedipine and tetrodotoxin, which are blockers of voltage-gated calcium and sodium channels, respectively, had only a small effect on the responses to increased temperature (fig. S1, H, J, K, and L). 2-aminoethoxydiphenyl borate (2-APB), a potent inhibitor of several ion channels and activator of TRPV-type channels (*28*–*30*), abolished the temperature response of POA neurons in a reversible manner (Fig. 1A).

[1]Department of Pharmacology, University of Heidelberg, Im Neuenheimer Feld 366, 69120 Heidelberg, Germany. [2]European Molecular Biology Laboratory (EMBL), Adriano Buzzati-Traverso Campus, Via Ramarini 32, 00016 Monterotondo, Italy. [3]Molecular Medicine Partnership Unit, EMBL, Meyerhofstraße 1, 69117 Heidelberg, Germany. *Present Address: Max Delbrück Center for Molecular Medicine, Robert Rössle Straße 10, 13125 Berlin, Germany. †These authors contributed equally to this work. **‡Corresponding author. Email: jan.siemens@pharma.uni-heidelberg.de**

Among known temperature-responsive ion channels, TRPC5, TRPM2, TRPM3, TRPM8, TRPV1, TRPV2, TRPV3, and STIM1-ORAI1 are sensitive to 2-APB (fig. S1M) (*24*–*26*). Because TRPC5 and TRPM8 are cold-sensitive channels (*31*–*33*), we eliminated them from our list of candidates. The STIM1-ORAI1 channel complex responds to cooling subsequent to a heat stimulus (*34*), a characteristic that differs from the POA responses described here.

The TRPV1 to -3 channels are activated rather than inhibited by 2-APB (*28*, *35*), and capsaicin, the cognate agonist of heat-sensitive TRPV1, did not have any effect on POA neurons (fig. S1N), suggesting that TRPV1 to -3 do not serve as temperature sensors in POA neurons. Moreover, these channels are sensitive to the pore blocker ruthenium red (*36*), a substance that had only a subtle effect on the temperature sensitivity of POA neurons (fig. S1, I and L).

TRPM3, one of the two remaining candidates, appeared to be expressed in the POA, albeit in low amounts, as assessed by in situ hybridization (fig. S1O). However, the TRPM3 agonist pregnenolone sulfate did not produce calcium responses in neuronal POA cultures (fig. S1N). It did so in dorsal root ganglia sensory neurons that express the receptor (*37*), which we used as a positive control.

Immunohistochemistry and in situ hybridization for TRPM2 showed prominent labeling within the mouse POA (Fig. 1, B and C, and fig. S3, B and C). H_2O_2, a sensitizer of TRPM2 channel activity (*38*), shifted the warm sensitivity of POA cultures to a lower activation temperature (Fig. 1D). Moreover, adenosine diphosphate ribose (ADPR), an intracellular agonist of TRPM2 (*39*, *40*), induced large currents in POA neurons that were identified by calcium imaging to be warm-sensitive (Fig. 1, E and F, and fig. S1, P to S). The ADPR-induced current showed a TRPM2-characteristic linear current-voltage relationship (*39*, *40*). Additionally, a similar current was induced in these neurons by increased temperatures (Fig. 1F).

Thus, TRPM2 may mediate responses to temperature increases in the POA. To test this, we used cultures obtained from *Trpm2*$^{-/-}$ mice (*41*) and compared their thermal responses with those from wild-type (*Trpm2*$^{+/+}$) littermate controls. The magnitude of the response of POA neurons to increased temperature was decreased in the absence of TRPM2, and these neurons were indistinguishable from warm-insensitive (non-WSN) *Trpm2*$^{+/+}$ POA neurons (Fig. 1, G and H). Using our stringent definition of warm sensitivity (fig. S1F), no responses to increased temperatures were detected in cultures obtained from *Trpm2*$^{-/-}$ mice (Fig. 1I).

The activation temperature of cultured WSNs—in the absence of a sensitizer such as H_2O_2 or any other reactive oxygen species—was in the range of 45°C (fig. S2A). Although this temperature is similar to that previously reported for TRPM2 activation (*38*), it exceeds any physiologically relevant deep brain temperature, even when compared with extreme forms of fever and hyperthermia (*42*). However, similar to other thermosensitive TRP channels, the activation temperature for TRPM2 appears not to be a fixed threshold temperature. Rather, it ranges from 33° to 47°C, depending on the cellular context (*38*, *43*). We therefore tested whether the activation temperature of POA neurons shifted to lower, more physiological temperatures when calcium imaging was performed on acutely obtained brain slices from 7- to 8-week-old mice. In this experimental setting, the neurons largely retained their native cellular environment and had attained maturity.

To this end, we injected virus particles into the mouse POA for Cre-dependent expression of the virally encoded intracellular calcium indicator GCaMP6, which shows increased fluorescence

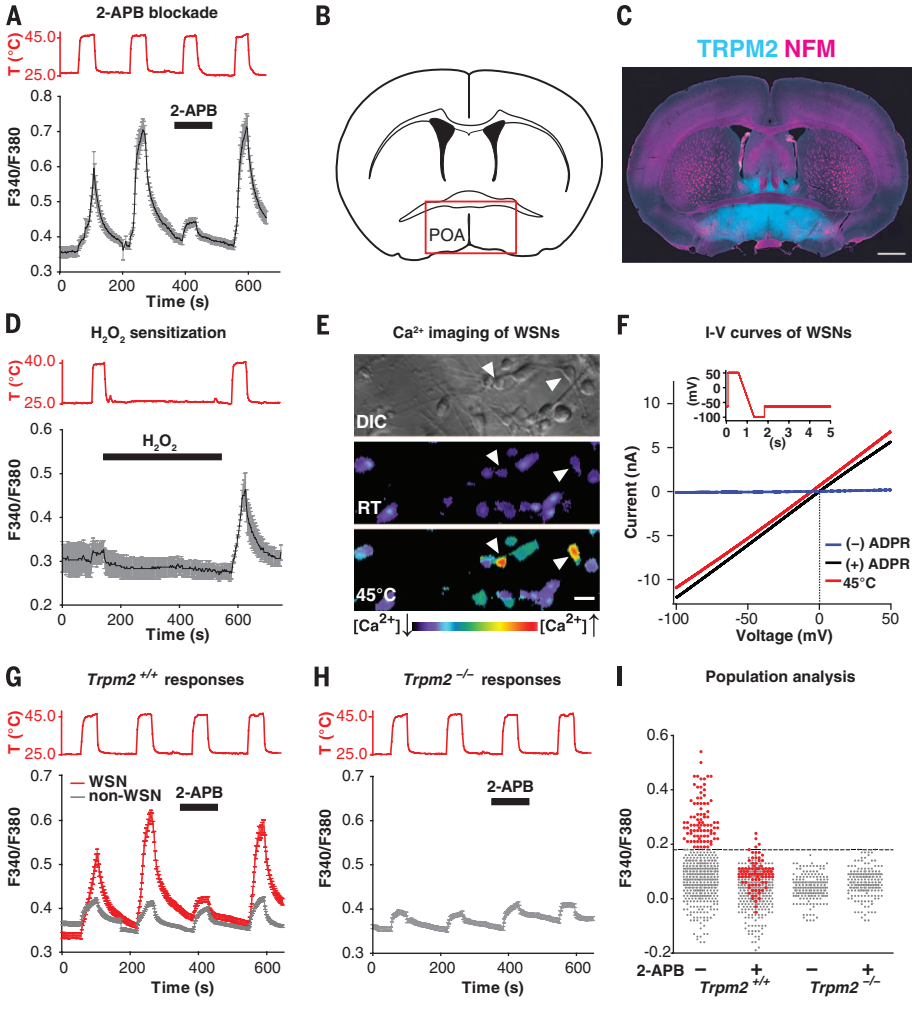

Fig. 1. TRPM2 mediates heat responses in a subset of POA neurons. (**A**) Cultured mouse POA neurons were examined for calcium responses [black trace; plotted are non-normalized fura-2 fluorescence intensity ratios after excitation at 340 and 380 nm (F340/F380)] to repetitive increases in temperature (red trace). 2-APB (30 μM, black bar) reversibly blocked thermal responses in POA neurons. (**B**) Cartoon depicting a coronal section of a mouse brain (Bregma level anterior-posterior, 0.14 mm). (**C**) Immunostaining of a representative mouse brain section corresponding to the cartoon in (B), using antibodies against TRPM2 (cyan) and neurofilament medium (NFM, magenta). Scale bar, 1 mm. (**D**) H_2O_2 (1 mM, black bar) sensitized POA neurons to respond to lower activation temperatures (40°C), as assessed by fura-2–based calcium imaging (black trace). (**E**) Differential interference contrast (DIC) image (top) and fura-2 ratio images before (middle; RT, room temperature) and during (bottom) a temperature stimulus of cultured POA neurons. Arrowheads indicate WSNs. (**F**) Current-voltage (*I-V*) relationships of voltage-clamped WSNs shown in (E) in response to a voltage ramp shown at the top, in the absence (blue) or presence (black) of ADPR (100 μM) or at a temperature stimulus of 45°C (red). (**G** and **H**) POA cultures from *Trpm2*$^{+/+}$ (G) and *Trpm2*$^{-/-}$ (H) mice were examined by calcium imaging for responses to repetitive thermal stimuli (upper red traces) in the presence or absence of 2-APB (30 μM, black bar). In *Trpm2*$^{+/+}$ cultures, both WSNs (red) and non-WSNs (light gray) could be detected, whereas WSNs were absent in cultures of *Trpm2*$^{-/-}$ mice. (**I**) Population analysis of thermal responses of POA neurons from *Trpm2*$^{+/+}$ and *Trpm2*$^{-/-}$ mice as shown in (G) and (H). Plotted are the peak responses of individual neurons at the second (without 2-APB) and third (with 2-APB) temperature stimulus. POA neurons of both genotypes had similar responses to a high-potassium solution (100 mM KCl, not shown). WSNs are colored in red and non-WSNs in gray. The dashed line demarcates the cutoff for warm sensitivity as defined in fig. S1F and table S1. Throughout, error bars indicate SEM.

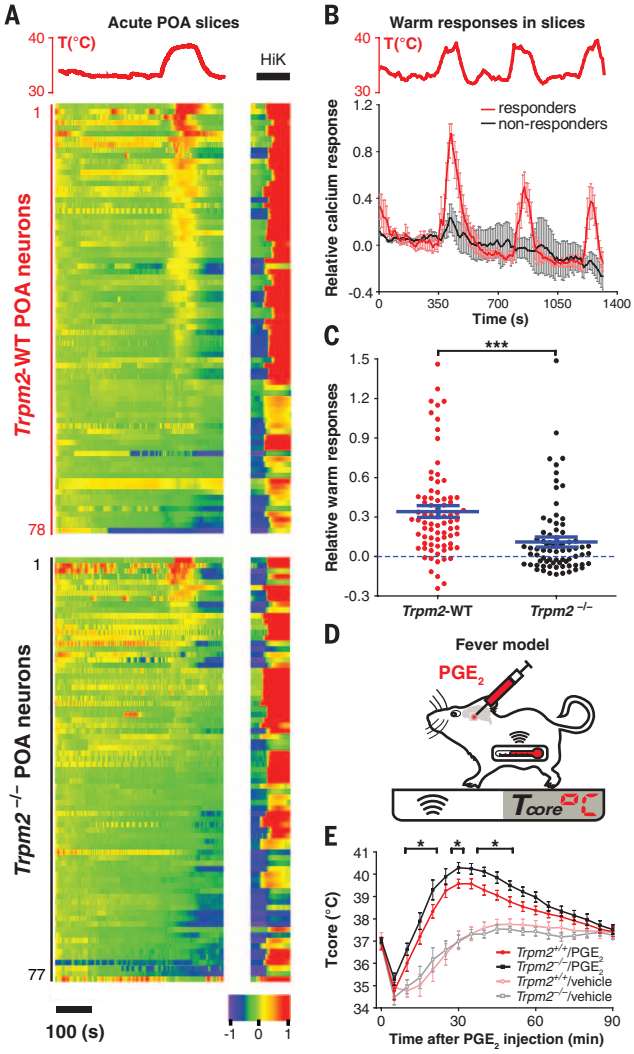

Fig. 2. TRPM2 mediates heat responses in POA brain slices and modulates fever temperature in vivo. (**A**) Acute POA slice preparations from *Nestin-Cre* mice with (*Trpm2*-WT; upper panel) or without (*Trpm2*$^{-/-}$; lower panel) functional TRPM2 were consecutively subjected to a temperature stimulus of 38 ± 1°C (red) and a high-potassium stimulus (HiK, black). Neuronal activity was recorded by means of a Cre-induced, virally encoded GCaMP6 calcium sensor that was stereotactically introduced into the POA 2 weeks before slice preparation. A nonlinear pseudocolor scale (bottom) indicates relative calcium responses in individual neurons. Numbering on the left refers to individual neurons. The black bar indicates the time scale. (**B**) Average relative calcium responses of exemplary GCaMP6^{+} WSNs (red; n = 5) and non-WSNs (black; n = 3) from *Nestin-Cre* mice to repetitive temperature stimuli of up to 40°C (top, red trace). (**C**) Population analysis of cellular responses shown in (A), demonstrating that relative heat-induced calcium signals are reduced in POA slices from mice lacking functional TRPM2 (***P < 0.0001, two-tailed Mann-Whitney test). Blue bars show the mean and SEM. (**D**) Cartoon depicting the experimental paradigm used to examine the fever response by thermotelemetrical measurements of T_{core} upon preoptic injection of PGE_2 into the POA. (**E**) Enhanced PGE_2-induced fever in *Trpm2*$^{-/-}$ mice (black trace; n = 9) compared with littermate *Trpm2*$^{+/+}$ controls (red trace; n = 10). Mice were briefly anesthetized to allow stereotactic injection of PGE_2 (or vehicle control), resulting in a transient drop of T_{core} for all conditions and genotypes. *P < 0.05, two-way analysis of variance (ANOVA) ($F_{1,318}$ = 40.78) followed by post hoc Fisher's least significant difference (LSD) test.

at 500 to 530 nm upon an increase in cytosolic calcium levels (*44*). To test temperature sensitivity in POA neurons, we used the neuron-specific *Nestin-Cre* mice (*45*) that express Cre recombinase, and thus GCaMP6, in POA neurons. Subsequent temperature stimulation of brain slices prepared from these animals revealed calcium responses in POA neurons at 38 ± 1°C (Fig. 2, A and B). Moreover, POA neurons in slices derived from mice lacking TRPM2 (*Nestin-Cre Trpm2*$^{-/-}$) had attenuated responses to the same temperature stimulus [mean relative heat responses ± SEM: *Nestin-Cre Trpm2*$^{-/-}$, 0.111 ± 0.033 (n = 78); *Nestin-Cre Trpm2*-WT, 0.341 ± 0.040 (n = 79); P < 0.0001, two-tailed Mann-Whitney test; *Trpm2*-WT signifies *Trpm2*$^{+/+}$ and *Trpm2*$^{+/-}$ mice] (Fig. 2, A and C, and fig. S2B). General excitability, as assessed by high potassium stimulation, was indistinguishable in the presence or absence of TRPM2 (fig. S2C). These results demonstrate that preoptic TRPM2 mediates responses to heat stress at temperatures of (or exceeding) 38°C.

Preoptic TRPM2 receptors modulate the magnitude of fever temperature

Fever is a cardinal response to infection and systemic inflammation. The POA, as part of its thermoregulatory function, is the key brain structure in controlling the increased body temperature in fever (*2*, *3*). The TRPM2-mediated activation of POA neurons at stimulation temperatures slightly above the physiological set point of 37°C (sometimes referred to as the balance point), might allow hypothalamic TRPM2 to detect and modulate inflammatory fever temperature.

As a consequence of infection and downstream of the resulting immune response, PGE_2 is the final mediator that triggers fever by acting directly on POA neurons (*2*, *46*). To address a putative fever-modulatory role for TRPM2 directly in the POA, we microinjected PGE_2 into this brain area in mice (Fig. 2D and fig. S2D), an established fever model (*46*–*48*). Telemetrically measured T_{core} revealed similar diurnal temperatures in the presence and absence of TRPM2 at normothermic (nonfever) conditions (fig. S2E). We found that injection of a low dose of PGE_2 (0.4 nmol per mouse) produced a mild fever response that was similar in both genotypes (fig. S2, F and I). However, a high dose of PGE_2 (4 nmol per mouse) caused an increased fever temperature in *Trpm2*$^{-/-}$ mice compared with that of *Trpm2*$^{+/+}$ littermate controls (Fig. 2E and fig. S2I). In the absence of functional TRPM2 protein, the maximal fever temperature reached 40.4 ± 0.2°C, compared with 39.6 ± 0.2°C in the presence of the receptor (n = 9 *Trpm2*$^{-/-}$ and 10 *Trpm2*$^{+/+}$ mice; P < 0.001, two-tailed unpaired t test).

We also tested the effects of the interleukins IL-1β and IL-6, which have been shown to synergistically induce fever at central sites (*49*). Again, significantly higher fever was detected in *Trpm2*$^{-/-}$ mice only for the stronger of the two stimuli, when both interleukins were co-injected into the POA, but not when IL-1β was injected alone (fig. S2, G to I). Together, these results indicate that preoptic TRPM2 limits the magnitude of the temperature increase in strong fever responses, presumably to prevent excessive temperature increases and tissue damage.

Trpm2-expressing POA neurons are part of a circuit controlling body temperature homeostasis

Our results indicated that *Trpm2*-expressing (*Trpm2*$^{+}$) neurons might be part of a thermoregulatory circuit and that TRPM2-driven activity might counteract body heating and perhaps promote peripheral heat loss at normothermic conditions as well. In the absence of specific agents to modulate TRPM2 function in vivo, we generated *Trpm2-2A-Cre* knock-in mice (referred to hereafter as *Trpm2-Cre* mice) that express Cre recombinase exclusively in *Trpm2*$^{+}$ cells (fig. S3A). We thereby gained genetic access to *Trpm2*$^{+}$ POA neurons and ascertained the potential thermoregulatory role of this specific cell population in unrestrained, conscious mice. We first assessed proper *Cre* expression in *Trpm2*$^{+}$ neurons, using in situ hybridization and *Cre* reporter mice. *Cre* was expressed in the POA of *Trpm2-Cre* mice, and its expression pattern recapitulated that of native *Trpm2* transcripts (fig. S3, B to F). Two-color in situ hybridization analysis of the POA revealed essentially complete cellular overlap of *Trpm2* and *Cre* (fig. S3F), with 97% of *Trpm2*$^{+}$ neurons (335 out of 344 cells) expressing the Cre-induced reporter.

We then tested whether modulating the activity of *Trpm2*$^{+}$ POA neurons influenced body temperature in freely moving mice. We chose a chemogenetic, DREADD (designer receptors exclusively activated by designer drugs) receptor–assisted approach that enabled us to remotely turn the activity of *Trpm2*$^{+}$ neurons on and off.

DREADDs are engineered heteromeric guanine nucleotide–binding protein (G protein)–coupled receptors that are activated by the otherwise inert drug clozapine-*N*-oxide (CNO) and couple to different G protein signaling cascades that either activate (Gq-DREADD) or inhibit (Gi-DREADD) neuronal activity (*50*). We injected viral constructs encoding Cre-dependent ("flexed") DREADD receptor expression cassettes (*51*) into the POA of *Trpm2-Cre* mice (Fig. 3A). This allowed the specific activation or inhibition of *Trpm2-Cre*$^+$ POA neurons through systemic application of CNO. No expression of DREADDs occurred in the absence of Cre recombinase.

To verify the capacity of CNO to exert control over *Trpm2*$^+$ neurons in vitro, we co-infected POA neurons by stereotactic injection of Cre-inducible DREADD receptors and GCaMP6 viral constructs into *Trpm2-Cre* mice. In brain slices derived from these mice, the respective DREADD receptor and GCaMP6 are coexpressed in *Trpm2*$^+$ neurons. Calcium imaging of POA neurons expressing Gq-DREADD or Gi-DREADD together with GCaMP6 confirmed that CNO application activated or inhibited *Trpm2*$^+$ neurons, respectively (fig. S3G).

We implanted telemetric temperature probes in the peritoneal cavity of DREADD-virus–injected *Trpm2-Cre* mice to permit recording of T_{core} in conscious, unrestrained animals (Fig. 3B). Diurnal body temperature regulation of DREADD-infected *Trpm2-Cre* mice in the absence of CNO was similar to that of control animals (fig. S3H). In contrast, CNO-mediated activation of *Trpm2*$^+$ POA neurons resulted in a sustained decrease in body temperature (Fig. 3, C to E, and fig. S3I). T_{core} dropped to 27.4 ± 0.6°C when *Trpm2*$^+$ neurons were activated in Gq-DREADD–infected mice but not in control-infected or saline-injected mice.

The temperature decrease correlated with a reduction in activity of the animals and was also reflected by a temperature drop of the body shell, as visualized by infrared (IR) imaging (Fig. 3F and movie S1). The hypothermic state lasted several hours (0.3 mg/kg of CNO induced hypothermia for 12.5 ± 2.4 hours) and could be induced repetitively without causing any apparent long-term adverse effects (Fig. 3E).

The animal's tail, an important thermal effector organ controlling heat dissipation (*3*, *52*), showed an increase in surface temperature of 3.7 ± 0.5°C that coincided with the overall heat loss (Fig. 3, F and G; fig. S3J; and movie S1), demonstrating that *Trpm2*$^+$ POA neurons drive hypothermia by triggering cutaneous vasodilation. Additionally, stimulation of *Trpm2*$^+$ neurons prevented activation of interscapular brown adipose tissue (BAT; fig. S3K), which normally mediates thermogenesis when the body cools.

Conversely, Gi-DREADD receptor–mediated inhibition of *Trpm2*$^+$ POA neurons resulted in a significant temperature increase, reaching a T_{core} of up to 39.1 ± 0.1°C (Fig. 3H and fig. S3I), suggesting that under normothermic conditions, *Trpm2*$^+$ neurons in the POA are tonically active. This is in agreement with previous electrophysiological recordings that show tonic ongoing activity of WSNs (*17*–*19*). Gi-DREADD–mediated neuronal inhibition had no significant effect on tail vasomotor tone at ambient temperature (~20°C), likely because the prominent vasoconstriction that prevails under these conditions (*53*) precludes detection of any further reduction of the IR signal (Fig. 3G). These results demonstrate that *Trpm2*$^+$ neurons in the POA are part of a circuit that orchestrates thermal effector processes to modulate T_{core} homeostasis.

Excitatory *Trpm2*$^+$ neurons drive hypothermia

WSNs in the POA have been proposed to be γ-aminobutyric acid (GABA)–releasing neurons that exert their effect largely by inhibiting downstream components of the thermoregulatory circuit (*3*). We therefore used two-color in situ hybridization on *Trpm2-Cre* reporter mice to ascertain whether *Trpm2*$^+$ neurons are of inhibitory or excitatory origin. We used in situ probes for transcripts encoding the vesicular glutamate transporter 2 (VGLUT2) and glutamate decarboxylase 1 (GAD1), which are excitatory and inhibitory markers, respectively (*54*) (Fig. 4A).

By this analysis, 30 ± 1% of *Trpm2*$^+$ POA neurons were excitatory (*Vglut2*$^+$) neurons, whereas 57 ± 7% coexpressed the inhibitory marker *Gad1* (mean ± SEM; n = 3 mice) (Fig. 4A and fig. S4A). We therefore tested whether activation of the excitatory or inhibitory neuronal population within the POA recapitulated the strong thermoregulatory phenotype observed on activation of *Trpm2*$^+$ neurons (Fig. 3, C to G). *Vgat-Cre* (*54*) and

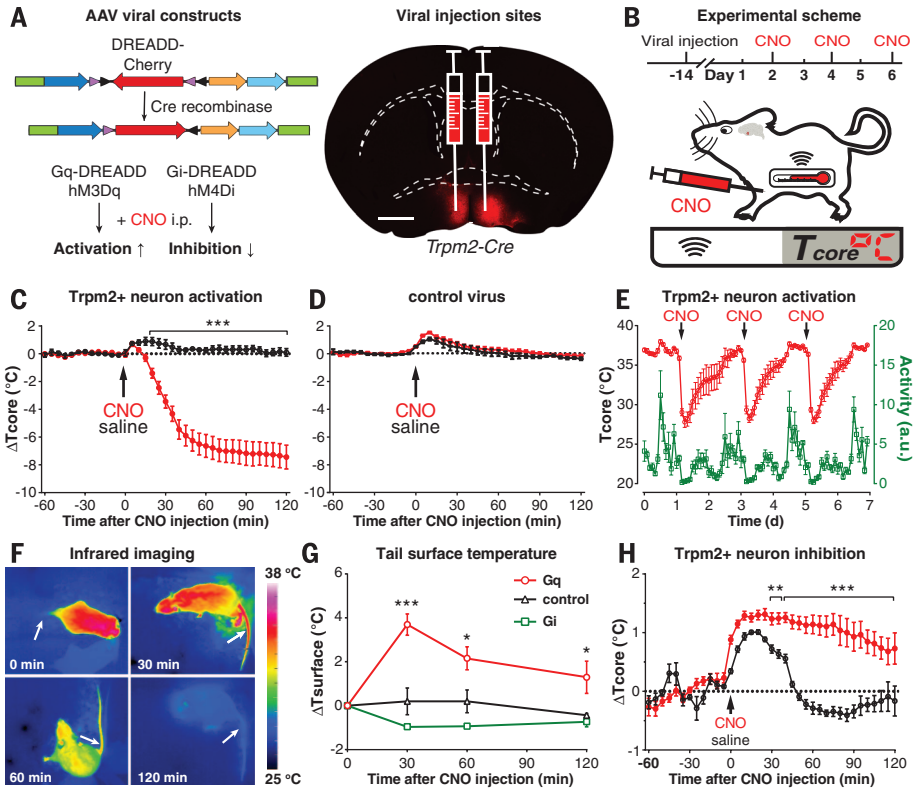

Fig. 3. Control of core body temperature by *Trpm2*$^+$ POA neuron activity. (**A**) Virally encoded, Cre-inducible DREADD-receptor–cherry fusion proteins (left panel) were bilaterally injected into the POA of *Trpm2-Cre* mice and visualized by fluorescent microscopy (right panel). The red arrows indicate the orientation of the DREADD–cherry cDNA reading frame; i.p., (injected) intraperitoneally. (**B**) Illustration detailing the experimental paradigm for examining the impact of *Trpm2*$^+$ neuronal activity on T_{core}. (**C** to **E**) CNO (0.3 mg/kg; red) or vehicle (saline; black) was intraperitoneally injected into mice infected with Gq-DREADD [(C) and (E)] or control virus (D), and T_{core} and activity [green trace in (E)] were measured telemetrically. Arrows indicate the time of injection. a.u., arbitrary units. (**F**) IR thermal imaging of *Trpm2-Cre* mice preoptically expressing Gq-DREADD in *Trpm2*$^+$ neurons, before (0 min) or at indicated time points after CNO injection, revealed pronounced cutaneous heat dissipation through tail vasodilation (arrows). (**G**) Change in tail temperature over time [(arrows in (F)] in *Trpm2-Cre* mice infected with Gq-DREADD (red), saline control (black), or Gi-DREADD (green) upon CNO treatment. (**H**) CNO-mediated inhibition of *Trpm2*$^+$ neurons in Gi-DREADD–infected *Trpm2-Cre* mice showed an oppositely directed effect compared with that in Gq-DREADD–infected animals (C) and resulted in a significant increase in T_{core}. The arrow indicates the time of injection. Telemetry data [(C), (D), and (H)]: Gq-DREADD $F_{1,6} = 75.6$, ***$P < 0.0001$; control virus $F_{1,6} = 1.55$; Gi-DREADD $F_{1,6} = 38.5$, **$P < 0.01$, ***$P < 0.0001$. IR imaging (G): Gq-DREADD $F_{1,5} = 9.3$, *$P < 0.05$, ***$P < 0.001$; Gi-DREADD $F_{1,4} = 5.2$; two-way ANOVA followed by post hoc Fisher's LSD test (n = 4 mice per group). P values indicate significance of the post hoc test.

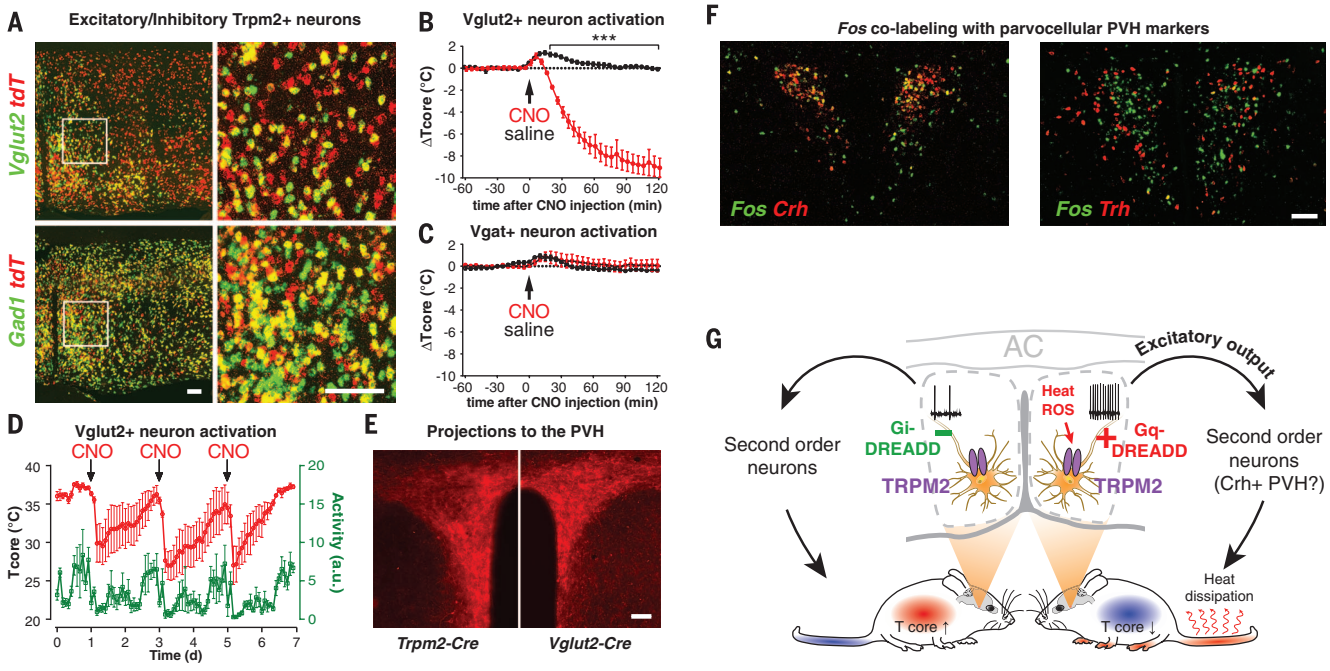

Fig. 4. Stimulation of preoptic *Vglut2*$^+$ neurons recapitulates *Trpm2*$^+$ neuron–driven hypothermia and activates *Crh*$^+$ neurons in the PVH. (**A**) Representative two-color in situ hybridizations of coronal brain sections from *Trpm2-Cre* mice crossed with a *Cre* reporter expressing *tdTomato* (*tdT*) with probes detecting *tdT* (red) and *Gad1* or *Vglut2* (green). The right panels show close-up views indicated by the boxes in the left panels. (**B** to **D**) *Vglut2-Cre* mice and *Vgat-Cre* mice were bilaterally injected with Gq-DREADD virus and subjected to the same experimental paradigm as shown in Fig. 3B. Arrows indicate the time of injection. CNO-mediated activation of *Vglut2-Cre* mice [(B) and (D)], but not *Vgat-Cre* mice (C), recapitulated *Trpm2*$^+$ neuron–driven hypothermia both in magnitude (B) and kinetics (D). *Vglut2-Cre* $F_{1,6} = 86.08$, $^{***}P < 0.0001$; *Vgat-Cre* $F_{1,4} = 0.44$; two-way ANOVA followed by post hoc Fisher's LSD test ($n = 4$ *Vglut2-Cre* and 3 *Vgat-Cre* mice). (**E**) Representative fluorescent images of brain sections from *Vglut2-Cre* and *Trpm2-Cre* mice preoptically expressing Gq-DREADD–cherry fusion protein (Fig. 3A), showing cherry$^+$ fibers projecting to the PVH. (**F**) Two-color fluorescent in situ hybridizations of brain sections from *Vglut2-Cre* mice preoptically expressing Gq-DREADD, using probes to detect *Fos* (green) and *Crh* or *Trh* (red). The animals were injected with CNO 30 minutes before preparation of the tissue sections. Neuronal activation of *Crh*$^+$ neurons but not *Trh*$^+$ neurons in the PVH was detected. (**G**) Model depicting *Trpm2*$^+$ POA neurons and their bidirectional effect on T_{core}. Heat (and reactive oxygen species, ROS) activate TRPM2 to depolarize WSNs, a process that can be mimicked by exogenous Gq-DREADD activation. Increased WSN activity (black traces) triggers an excitatory pathway that promotes heat loss and hypothermia, possibly through a circuit involving *Crh*$^+$ neurons in the PVH. Conversely, inhibiting *Trpm2*$^+$ neurons results in an elevation of T_{core}. AC, anterior commissure. *P* values indicate significance of the post hoc test. All scale bars, 100 μm.

Vglut2-Cre (*55*) mice have been used previously to label inhibitory and excitatory hypothalamic neurons, respectively. Thus, T_{core} recordings of Gq-DREADD–injected *Vgat-Cre* and *Vglut2-Cre* mice were acquired, and viral expression in the respective POA neurons was later verified (fig. S4, B and C). CNO activation of *Vglut2*$^+$ neurons but not *Vgat*$^+$ neurons reproduced the prolonged drop in T_{core} (Fig. 4, B to D), indicating that excitatory, *Trpm2*$^+$ neurons mediate the strong thermoregulatory effect. *Vglut2*$^+$ neuron–driven hypothermia could be induced repetitively and was well tolerated by the animals (Fig. 4D), similar to observations for in vivo chemogenetic activation of preoptic *Trpm2*$^+$ neurons (Fig. 3E). In situ hybridization revealed that Cre recombinase in the *Vglut2-Cre* line was expressed only in ~20% of all *Vglut2*$^+$ POA neurons (fig. S4D). This indicates that activation of a subpopulation of *Vglut2*$^+$ POA neurons, making up only ~6% of all preoptic *Trpm2*$^+$ neurons (fig. S4A), is sufficient to mediate the strong hypothermic effect (Fig. 4, B and D).

Thermoregulatory signals arising from the POA are channeled to different peripheral effector organs through discrete hypothalamic and extrahypothalamic output nuclei (*3*). Given the overlapping expression pattern of *Vglut2* and *Trpm2* in the POA and a similar capacity of both neuron groups to trigger hypothermia on activation, we reasoned that axons of both neuron cohorts might converge on the same downstream output nucleus. Projections of *Cre*-expressing POA neurons were labeled with fluorescent reporters that were introduced together with the DREADD expression cassette by viral infection of the POA area (Fig. 3A). POA infections of *Trpm2-Cre* and *Vglut2-Cre* mice resulted in prominent labeling of fibers terminating in the paraventricular nucleus of the hypothalamus (PVH) (Fig. 4E), a region not previously identified as a major thermoregulatory outlet (*3*). Moreover, CNO administration in *Trpm2-Cre* and *Vglut2-Cre* mice harboring Gq-DREADD–infected POA neurons resulted in DREADD-specific expression of *Fos* in the PVH, demonstrating that *Trpm2*$^+$ *Vglut2*$^+$ POA neurons can excite PVH neurons (fig. S4E). Corticotropin-releasing hormone–positive (*Crh*$^+$) neurons in the PVH are part of the hypothalamic-pituitary-adrenal (HPA) stress response system, which is also activated in response to fever (*56*). We found that DREADD-mediated activation of *Vglut2*$^+$ POA neurons specifically excites parvocellular *Crh*$^+$ neurons but not neighboring thyrotropin-releasing hormone–positive (*Trh*$^+$) neurons or magnocellular vasopressin$^+$ and oxytocin$^+$ PVH neurons (Fig. 4F and fig. S4F). Of all *Fos*$^+$ neurons, we found that 88.4 ± 1.5% (mean ± SEM; $n = 3$ mice) are *Crh*$^+$.

Collectively, these results indicate that *Trpm2*$^+$ *Vglut2*$^+$ POA neurons detect increased body temperature and initiate thermoregulatory defense mechanisms, putatively through activation of stress-responsive *Crh*$^+$ neurons in the PVH (Fig. 4G).

Discussion

Explanations of the molecular mechanisms mediating thermal detection in preoptic WSNs have remained speculative (*57*, *58*). We identified TRPM2 as a thermal sensor in a subset of POA neurons that are part of a circuit controlling T_{core}.

Preoptic TRPM2 was activated at temperatures above the physiological set point of 37°C, arguing for a function of this receptor at conditions of elevated core temperatures and heat stress. Our results demonstrate a role for preoptic TRPM2 in regulating the magnitude of the fever response, suggesting that heightened temperatures, potentially

together with reactive oxygen species that are produced under these conditions (*59*), activate the channel to promote heat loss and prevent overheating.

Fever temperatures activate the immune system to modulate inflammatory responses (*60*). TRPM2 is expressed in the immune system (*61*), suggesting that fever-activated TRPM2 might modulate immune cell function. TRPM2 activity has been shown to inhibit and counteract inflammatory (pyrogenic) signaling in phagocytes (*62*), paralleling our results and emphasizing a convergent TRPM2-based mechanism used by both the immune and nervous systems to limit the extent of an inflammatory response and the mediation of antipyresis.

We observed a TRPM2-mediated reduction in T_{core} only when strong fever responses were induced, suggesting that TRPM2 limits the upper fever range and acts as an "emergency break" to prevent overheating and tissue damage. Alternatively, it is possible that TRPM2 plays a more prominent role in fever regulation, but that this function is masked by compensatory mechanisms triggered in *Trpm2*$^{-/-}$ mice that ubiquitously lack this ion channel throughout development.

The current model of thermoregulation predicts that the action potential firing rate of WSNs in the POA underlies T_{core} homeostasis and controls peripheral autonomous thermal responses (*3*). We found that chemogenetic activation and inhibition of *Trpm2*$^{+}$ WSNs in mice results in hypo- and hyperthermia, respectively, providing direct in vivo evidence for the validity of this hypothesis.

Twenty to 40% of POA neurons are sensitive to temperature and respond to stimuli around 37°C in electrophysiological experiments (*17*). Using calcium imaging, we found that only around 16% of neurons responded to a temperature increase. It is possible that our approach only allowed the detection of neurons that robustly responded to a thermal stimulus. Buffering of intracellular free calcium by the calcium indicators used in our experiments is one possible explanation for the reduced sensitivity and might explain the lower percentage of responsive neurons. Our data indicate that the TRPM2 receptor is unlikely to account for temperature sensitivity at normothermia but rather detects heat stress above 37°C. Accordingly, in POA brain slices, some thermal responses were still detectable in the absence of TRPM2, implying that additional mechanisms mediate preoptic responses to warming. Given the relatively broad expression of TRPM2 in the POA, it is plausible that the receptor covers detection of the upper, pathological temperature range in many or even all WSNs.

Previous single-cell transcriptome analysis has shown that preoptic WSNs are unexpectedly heterogeneous (*63*). Nevertheless, WSNs have been found to largely be inhibitory (GABAergic) neurons, which is in agreement with our histochemical analysis (summarized in fig. S4A). However, because the hypothermic phenotype that we observed in *Trpm2-Cre* mice was recapitulated by activating the smaller subpopulation of excitatory *Vglut2*$^{+}$ neurons but not by activating inhibitory (*Vgat*$^{+}$) neurons, we focused on the excitatory branch of the *Trpm2*$^{+}$ population. We found that preoptic *Vglut2*$^{+}$ neurons project to and excite *Crh*$^{+}$ neurons in the PVH, a hypothalamic cell population that is not primarily associated with thermoregulation (*3*), but rather controls stress reactions including fever responses by activation of the HPA axis. Excitation of PVH neurons inhibits PGE_2-induced fever (*47*). Moreover, corticosterone release by HPA axis activation has been found to counteract and reduce fever responses (*64*, *65*). These findings are in agreement with our data. The TRPM2 receptor may curtail PGE_2-triggered fever and induce hypothermia by mediating monosynaptic excitation of *Crh*$^{+}$ neurons in the PVH through an excitatory thermoregulatory pathway that connects the POA with the HPA axis.

Our study delineates a genetic framework for dissecting the central pathways controlling temperature homeostasis and provides a way to remotely control core body temperature in conscious, unrestrained mice by chemogenetic manipulation of the hypothalamic thermostat. These hypo- and hyperthermic model systems may help in exploring the effects of altered core body temperature on diverse processes such as trauma recovery, immune modulation, energy expenditure, obesity, and longevity.

REFERENCES AND NOTES

1. T. Bartfai, B. Conti, *Sci. World J.* **10**, 490–503 (2010).
2. C. B. Saper, A. A. Romanovsky, T. E. Scammell, *Nat. Neurosci.* **15**, 1088–1095 (2012).
3. S. F. Morrison, *Auton. Neurosci.* **196**, 14–24 (2016).
4. M. E. Musselman, S. Saely, *Am. J. Health Syst. Pharm.* **70**, 34–42 (2013).
5. W. D. Dietrich, H. M. Bramlett, *Brain Res.* **1640**, 94–103 (2016).
6. T. C. Wu, J. C. Grotta, *Lancet Neurol.* **12**, 275–284 (2013).
7. T. L. Horvath, N. S. Stachenfeld, S. Diano, *Yale J. Biol. Med.* **87**, 149–158 (2014).
8. H. C. Heller, L. I. Crawshaw, H. T. Hammel, *Sci. Am.* **239**, 102–110, 112–113 (1978).
9. B. A. Baldwin, D. L. Ingram, *J. Physiol.* **191**, 375–392 (1967).
10. H. T. Hammel, J. D. Hardy, M. M. Fusco, *Am. J. Physiol.* **198**, 481–486 (1960).
11. H. W. Magoun, F. Harrison, J. R. Brobeck, S. W. Ranson, *J. Neurophysiol.* **1**, 101–114 (1938).
12. E. Satinoff, *Am. J. Physiol.* **206**, 1389–1394 (1964).
13. B. Folkow, G. Strom, B. Uvnas, *Acta Physiol. Scand.* **17**, 317–326 (1949).
14. B. Conti *et al.*, *Science* **314**, 825–828 (2006).
15. M. M. Fusco, J. D. Hardy, H. T. Hammel, *Am. J. Physiol.* **200**, 572–580 (1961).
16. H. C. Heller, *Experientia Suppl.* **32**, 267–276 (1978).
17. J. A. Boulant, *J. Appl. Physiol.* **100**, 1347–1354 (2006).
18. T. Nakayama, J. S. Eisenman, J. D. Hardy, *Science* **134**, 560–561 (1961).
19. T. Nakayama, H. T. Hammel, J. D. Hardy, J. S. Eisenman, *Am. J. Physiol.* **204**, 1122–1126 (1963).
20. A. E. Oliver, G. A. Baker, R. D. Fugate, F. Tablin, J. H. Crowe, *Biophys. J.* **78**, 2116–2126 (2000).
21. C. Cai, X. Meng, J. He, H. Wu, F. Zou, *Neurosci. Lett.* **506**, 336–341 (2012).
22. I. V. Tabarean, B. Conti, M. Behrens, H. Korn, T. Bartfai, *Neuroscience* **135**, 433–449 (2005).
23. J. A. Boulant, J. B. Dean, *Annu. Rev. Physiol.* **48**, 639–654 (1986).
24. R. Palkar, E. K. Lippoldt, D. D. McKemy, *Curr. Opin. Neurobiol.* **34**, 14–19 (2015).
25. J. Vriens, B. Nilius, T. Voets, *Nat. Rev. Neurosci.* **15**, 573–589 (2014).
26. H. Wang, J. Siemens, *Temperature* **2**, 178–187 (2015).
27. L. Vay, C. Gu, P. A. McNaughton, *Br. J. Pharmacol.* **165**, 787–801 (2012).
28. H. Z. Hu *et al.*, *J. Biol. Chem.* **279**, 35741–35748 (2004).
29. K. Togashi, H. Inada, M. Tominaga, *Br. J. Pharmacol.* **153**, 1324–1330 (2008).
30. S. Z. Xu *et al.*, *Br. J. Pharmacol.* **145**, 405–414 (2005).
31. D. M. Bautista *et al.*, *Nature* **448**, 204–208 (2007).
32. A. Dhaka *et al.*, *Neuron* **54**, 371–378 (2007).
33. K. Zimmermann *et al.*, *Proc. Natl. Acad. Sci. U.S.A.* **108**, 18114–18119 (2011).
34. B. Xiao, B. Coste, J. Mathur, A. Patapoutian, *Nat. Chem. Biol.* **7**, 351–358 (2011).
35. J. Siemens *et al.*, *Nature* **444**, 208–212 (2006).
36. D. E. Clapham, C. Montell, G. Schultz, D. Julius, *Pharmacol. Rev.* **55**, 591–596 (2003).
37. J. Vriens *et al.*, *Neuron* **70**, 482–494 (2011).
38. M. Kashio *et al.*, *Proc. Natl. Acad. Sci. U.S.A.* **109**, 6745–6750 (2012).
39. A. L. Perraud *et al.*, *Nature* **411**, 595–599 (2001).
40. Y. Sano *et al.*, *Science* **293**, 1327–1330 (2001).
41. S. Yamamoto *et al.*, *Nat. Med.* **14**, 738–747 (2008).
42. W. P. Cheshire Jr., *Auton. Neurosci.* **196**, 91–104 (2016).
43. K. Togashi *et al.*, *EMBO J.* **25**, 1804–1815 (2006).
44. T. W. Chen *et al.*, *Nature* **499**, 295–300 (2013).
45. F. Tronche *et al.*, *Nat. Genet.* **23**, 99–103 (1999).
46. M. Lazarus *et al.*, *Nat. Neurosci.* **10**, 1131–1133 (2007).
47. C. J. Madden, S. F. Morrison, *Am. J. Physiol. Regul. Integr. Comp. Physiol.* **296**, R831–R843 (2009).
48. T. E. Scammell, J. K. Elmquist, J. D. Griffin, C. B. Saper, *J. Neurosci.* **16**, 6246–6254 (1996).
49. L. M. Harden, I. du Plessis, S. Poole, H. P. Laburn, *Brain Behav. Immun.* **22**, 838–849 (2008).
50. B. L. Roth, *Neuron* **89**, 683–694 (2016).
51. M. Koch *et al.*, *Nature* **519**, 45–50 (2015).
52. R. M. McAllen, M. Tanaka, Y. Ootsuka, M. J. McKinley, *Eur. J. Appl. Physiol.* **109**, 27–33 (2010).
53. C. J. Gordon, *Temperature Regulation in Laboratory Rodents* (Cambridge Univ. Press, 1993).
54. L. Vong *et al.*, *Neuron* **71**, 142–154 (2011).
55. L. Borgius, C. E. Restrepo, R. N. Leao, N. Saleh, O. Kiehn, *Mol. Cell. Neurosci.* **45**, 245–257 (2010).
56. Y. Matsuoka *et al.*, *Proc. Natl. Acad. Sci. U.S.A.* **100**, 4132–4137 (2003).
57. J. A. Boulant, *Am. J. Physiol. Regul. Integr. Comp. Physiol.* **290**, R1481–R1484, discussion R1484 (2006).
58. S. Kobayashi, A. Hori, K. Matsumura, H. Hosokawa, *Am. J. Physiol. Regul. Integr. Comp. Physiol.* **290**, R1479–R1480, discussion R1484 (2006).
59. W. Riedel, G. Maulik, *Mol. Cell. Biochem.* **196**, 125–132 (1999).
60. S. S. Evans, E. A. Repasky, D. T. Fisher, *Nat. Rev. Immunol.* **15**, 335–349 (2015).
61. H. Knowles, Y. Li, A. L. Perraud, *Immunol. Res.* **55**, 241–248 (2013).
62. A. Di *et al.*, *Nat. Immunol.* **13**, 29–34 (2012).
63. J. Eberwine, T. Bartfai, *Pharmacol. Ther.* **129**, 241–259 (2011).
64. I. Chowers, N. Conforti, S. Feldman, *Am. J. Physiol.* **214**, 538–542 (1968).
65. J. L. McClellan, J. J. Klir, L. E. Morrow, M. J. Kluger, *Am. J. Physiol.* **267**, R705–R711 (1994).

ACKNOWLEDGMENTS

We thank Y. Mori for *Trpm2*$^{-/-}$ mice and TRPM2 antisera; B. Lowell for *Vgat-Cre* mice; members of R. Kuner's laboratory, the Nikon Imaging Center, and V. Grinevich for sharing reagents, equipment, and expertise; A. von Seggern and C. Steinmeyer-Stannek for technical support; K. Schrenk-Siemens, W. de Lima, and P. Bengtson for help with calcium imaging; and C. Bohlen and A. Littlewood-Evans for criticism and reading of the manuscript. All data necessary to understand the study and its conclusions are in the body of the manuscript and in the supplementary materials. All primary data are archived on secure servers at the University Hospital Heidelberg. All data will be made available upon request. This work was supported by the European Research Council (grant ERC-2011-StG-280565 to J.S.), the Alexander von Humboldt Foundation (German Federal Ministry for Education and Research, BMBF; fellowship to G.B.K. and grant to J.S.), and the German Research Foundation (grants as part of the Collaborative Research Center SFB-1158 to P.H. and J.S.). Additional support came from the CellNetworks Cluster of Excellence. J.S., together with K.S., H.Wa., and G.B.K., conceived the project and designed the experiments. K.S. designed and conducted the cellular screen and analysis; J.P. designed and performed electrophysiological experiments; G.B.K. conceived the slice physiology and fever experiments; and H.Wa. conceived and conducted the chemogenetic experiments and, together with H.We., P.H., and F.d.C.R., generated *Trpm2-Cre* mice. H.We. and H.Wa. conducted histochemical analysis. J.S. wrote the paper. All authors commented on and approved the paper.

SUPPLEMENTARY MATERIALS

www.sciencemag.org/content/353/6306/1393/suppl/DC1
Materials and Methods
Figs. S1 to S4
Table S1
References (*66*–*76*)
Movie S1

24 March 2016; accepted 27 July 2016
Published online 25 August 2016
10.1126/science.aaf7537

www.sciencemag.org/cgi/content/full/science.aaf7537/DC1

Supplementary Materials for

The TRPM2 channel is a hypothalamic heat sensor that limits fever and can drive hypothermia

Kun Song,* Hong Wang,* Gretel B. Kamm,* Jörg Pohle, Fernanda de Castro Reis, Paul Heppenstall, Hagen Wende, Jan Siemens†

*These authors contributed equally to this work.
†Corresponding author. E-mail: jan.siemens@pharma.uni-heidelberg.de

Published 25 August 2016 on *Science* First Release
DOI: 10.1126/science.aaf7537

This PDF file includes:

Other Supplementary Material for this manuscript includes the following:
(available at www.sciencemag.org/cgi/content/full/science.aaf7537/DC1)

Supplementary Materials

Material and Methods

Animals

Animal housing and experimentation was in accordance with the local animal welfare and use guidelines (Regierungspräsidium Karlsruhe, Germany).

We generated *Trpm2-Cre* mice using recombineering techniques as described previously (*66*). In brief, an 8.3 kbp region flanking *Trpm2* exon 34 was retrieved from BAC clone RP23-13818. A selection cassette containing a T2A sequence (*67*) linked to iCre-recombinase (*68*) and a FRT-flanked neomycin resistance gene was inserted upstream of the stop codon of the *Trpm2* gene (fig. S3A left panel). The final targeting vector was linearized by NotI, electroporated into A9 (129/C57Bl6-derived hybrid-) ES cells (EMBL Mouse Biology Unit, Monterotondo). Individual ES cell clones were identified by southern blot (fig. S3A, middle panel). A positive clone was injected into 8-cell stage embryos to generate founder mice heterozygous for the targeted allele. Founder males were crossed with FLPeR-expressing transgenic females (*69*) to remove the FRT flanked neomycin cassette. *Trpm2-Cre* mice were kept on a C57BL/6N background and heterozygous animals were used for experiments. The genotype of *Trpm2-Cre* animals was verified by PCR with primers flanking the 2A-Cre cassette (P1 5'-GATCCCTCTGTATGCGAACC-3', P2 5'- AAAGCATGGCACTTGAGGACATA-3') (FigS3A right panel).

Nestin-Cre, *Vglut2-Cre*, *Vgat-Cre*, *Trpm2*$^{-/-}$, *Ai9* and *Z/AP* mouse lines have been derived previously (*41, 45, 54, 55, 70, 71*).

For all *in vivo* experiments examining autonomous functions (T_{core} measurements, IR recordings, mouse activity), both male and female mice were used. The animals were randomly assigned for experiments. The experimenters were aware of the animals' genotype when conducting experiments.

1. Primary neuronal culture and Calcium-imaging

1.1 Primary preoptic neuronal cultures

Preoptic neurons were isolated from brains of 1-3 day old postnatal C57Bl/6N mouse pups purchased from Charles River Laboratories. In brief, brains were isolated quickly, and 200 μm thick brain slices containing the preoptic area of the hypothalamus were cut on a vibratome (HM650V, Thermo Scientific, USA) in artificial cerebral spinal fluid (ACSF; in mM: 135.5 NaCl, 1 KCl, 2 $CaCl_2$, 1.3 $MgCl_2$, 1.26 K_2HPO_4, 26 $NaHCO_3$ and 9 glucose oxygenized in carbogen (95% O_2 and 5% CO_2). The preoptic area was micro-dissected from each brain slice in HBSS solution (Invitrogen, USA). Small POA tissue pieces were collected under microscopic control and incubated in HBSS solution containing 0.5 mg/ml papain at 37 °C for 20 min. After the digestion procedure, the tissue was mechanically dissociated into a single-cell suspension by trituration in neurobasal medium (Invitrogen, USA) with a glass pasteur pipette. After centrifugation (300 g, 5 min), the cell pellet was resuspended in neurobasal medium and plated on coverslips sequentially coated with poly-D-lysine (Sigma, USA) and laminin (Sigma, USA). The isolated POA neurons were cultured in a humidified incubator at 37 °C, 5% CO_2 for two days before imaging.

1.2 Calcium-imaging of primary preoptic neuronal cells

Cells in culture were first washed once with Ringer's solution (in mM) 140 NaCl, 5 KCl, 2 $CaCl_2$, 2 $MgCl_2$, 10 glucose, and 10 HEPES pH=7.4) and then incubated with 10 μM of the Ca^{2+}-sensitive ratiometric fluorescent dye Fura-2 AM (F1201; Molecular Probes, USA) for 90 min at RT in Ringer's solution. After the loading procedure, coverslips were mounted in a perfusion chamber (RC-22; Warner Instruments, USA) and perfused by an 8-channel modular perfusion system (ValveBank-8; AutoMate Scientific, USA). Calcium-imaging was performed using an inverted fluorescent microscope (Axio Vert.A1; Carl Zeiss, Germany) equipped with a 10X objective (Fluar 10X/0.5 M27, Carl Zeiss, Germany) and a cooled CCD camera (CoolSNAP-HQ2; Photometrics, USA). Fura-2 AM loaded cells were excited at the wavelengths of 340 nm and 380 nm (Chroma Fura-2 filter set), and the fluorescence was collected at 510 nm. The obtained images were analyzed for changes in the fluorescence intensity within regions of interest (ROIs) using MetaFluor 7.1 (Molecular Devices, USA). The intracellular calcium level $[Ca^{2+}]_i$ was represented as the fluorescence ratio F340/F380. The calcium-free Ringer's solution was prepared by substituting $MgCl_2$ for $CaCl_2$ at the same concentration and adding 2 mM EGTA. To change the temperature of the perfusion solution for the application of heating or cooling stimuli, Ringer's solution flowed through a glass coil with a custom-made thermal jacket surrounding it. A circulating water bath with heating/cooling function (MultiTemp III; Pharmacia Biotech, Sweden) pumped water into the jacket, allowing rapid and highly reproducible heat exchange with the perfusate (Ringer's solution). The bath temperature in the perfusion chamber was monitored by a thermocouple probe (IT-18; Physitemp Instruments, USA) connected with a digital

thermometer (BAT-12;Physitemp Instruments, USA). The bath temperature was simultaneously recorded along with the calcium signals.

For the statistical analysis of the heat responses using calcium-imaging data and for defining the cut-off value for warm-sensitive neurons (WSNs), calcium responses of individual cultured mouse POA neurons or HEK293 cells were calculated according to the difference between the basal ratio at room temperature (~ 24°C) and the peak ratio during a thermal stimulus of up to 45°C using Clampfit software (Ver.10.3). In brief, the initial fluorescence ratio F340/F380 for each cell at time point 0 was taken as the relative basal calcium level (R_0) at room temperature. Next, the peak ratio F340/F380 during the thermal stimulus (R_T) was determined for each cell. The response magnitude during the thermal stimulus was calculated by the formula $R_{\Delta T}=R_T-R_0$. Unspecific temperature dependent fluorescent changes of Fura-2 were accounted for by averaging $R_{\Delta T}$ Fura-2 signals of thermally unresponsive HEK293 cells and determining the mean + 5-times Standard Deviation (5SD). This value corresponded to a relative Fura-2 Ratio of $R_{\Delta T}=0.18$ (see Table S1 and fig. S1E, F for details).

1.3 Electrophysiological recordings of cultured primary preoptic area neurons

Cultures of preoptic area neurons were prepared as described above (see section 1.1). Differential interference contrast images were acquired with a 20X objective, F340/F380 calcium imaging was performed with a 10X objective (Fig. 1E). Using an inverted microscope, a diamond-shaped recording chamber was constantly perfused (~2 ml/min) with a gravity-driven ValveLink 8.2-system (AutoMate Scientific, USA) with (in mM)

136 NaCl, 4 KCl, 2 $CaCl_2$, 1 $MgCl_2$, 10 glucose and 10 HEPES, pH=7.4 with NaOH at room temperature, ~295 mOsm. Recordings were performed at room temperature. One to three heat stimuli of 45 °C and ~30 s duration were applied with pre-heated channels of the perfusion system. Robust Ca^{2+} responders were patched in whole-cell mode with an Axopatch 200B amplifier, sampled at 20 kHz, low pass filtered at 5 or 10 kHz and digitized with a Digidata 1440A using Clampex 10.6. Patch pipette solution contained (in mM) 0.1 or 10 EGTA, 10 HEPES, ~120 CsCl, 2 NaCl, 2 TEA-Cl, 1 $MgCl_2$, 6 Na_2-phosphocreatine, 3 Mg-ATP, 0.3 Na-GTP and 0 or 0.1 ADP-ribose (Sigma-Aldrich, A0752), pH 7.35 with CsOH at room temperature, ~275 mOsm. Open patch pipette resistance was ~4 MΩ, subsequent gigaseal ~5 GΩ. Neurons were held at -65 mV in voltage clamp. In order to inactivate voltage-gated sodium and calcium currents, the cells were depolarized to +50 mV for 500 ms before a ramp to -100 mV was applied within 750 ms to record current-voltage curves, (inset in fig. 1F). After 500 ms at -100 mV, the neuron was held again at -65 mV and holding current was recorded. The ramp protocol was repeated every 5 s.

The neurons were either patched with or without 0.1 mM ADP-ribose in the patch pipette solution. Cell capacity was measured directly after establishing whole-cell mode by applying voltage steps and averaging ≥ 5 current responses. If a current of at least -1 nA developed at -100 mV within 10 min in whole-cell mode, the neurons were counted as responders to ADP-ribose and ~10-20 ramps of the stable peak current were averaged. Cells patched without ADP-ribose were recorded for at least 10 min. For non-responders and control cells, the ramps of the last two minutes of the 10 min interval were averaged (fig. S1R and S).

Sodium-free extracellular solution consisted of (in mM) 136 NMDG, 4 KCl, 2 $CaCl_2$, 1 $MgCl_2$, 12 glucose and 10 HEPES, pH=7.4 with HCl at room temperature, ~295 mOsm. Analysis was carried out in Igor Pro 6.37 (WaveMetrics, USA), after importing Axon binary files with the DataAccess (Bruxton Corporation, USA). For the example trace in fig. S1P, the holding current was resampled with 1 kHz, plotted over time and completed by linear splines. No corrections were made for junction potentials. Conductance was measured by the slope of a linear fit to the respective I-V-curve.

2. Viral injections and calcium-imaging in brain slices

2.1 Stereotactic viral injections

Stereotactic injections were performed as previously described (*72*). Surgical procedures were performed aseptically. Mice were deeply anesthetized by an intraperitoneal (i.p.) injection of "sleep-mix" containing metedomidin (0.5 mg/kg), midazolam (5 mg/kg) and fentanyl (0.05 mg/kg). Fur on the head was removed by depilatory cream and eyes were protected by an eye ointment (Bepanthen; Bayer, Germany). Mice were placed on a stereotaxic apparatus (Kopf Model 1900; Tujunga, USA). After exposing a minimal area of the skull, a small hole of 0.2 mm diameter was drilled with a frame-mounted drill (Kopf 1911; Tujunga, USA) for injection. A pulled glass pipette with 20–40 µm tip diameter was inserted into the brain and virus was injected by an air pressure system. 100-200 nl of the recombinant adeno-associated virus encoding the Cre-dependent calcium indicator GCaMP6s (*44*) under control of the human synapsin-1 promoter (AAV1.Syn.Flex.GCaMP6s.WPRE.SV40, purchased from the University of

Pennsylvania Gene Therapy Program Vector Core) was injected unilaterally into the POA with the coordinates, Bregma: ML: 0.300 mm, AP: 0.000 mm and DV: -5.300 mm. After viral injection, the scalp was carefully sutured with sterile absorbable-needled sutures (Marlin® 17241041; Catgut, Germany). During the whole operation procedure, mice were kept on a 37 °C heating pad. Once the surgery was finished, the anesthesia was antagonized using a subcutaneous injection of "wakeup-mix" (antipamezol 2.5 mg/kg, flumazin 0.5 mg/kg and naloxon 1.2 mg/kg). After the surgery, mice were transferred to their home cages and exposed to infrared warming overnight to help recovery from the surgery. For postoperative care, mice were injected subcutaneously with carprofen (5 mg/kg, Rimadyl; Zoetis, USA). Brain slices were prepared for calcium-imaging two weeks after viral injection.

2.2 Calcium-imaging of acute brain slices

Nestin-Cre$^{+/-}$;*Trpm2-WT* and *Nestin-Cre*$^{+/-}$;*Trpm2*$^{-/-}$ mice aged between P47 and P60 were used in this experiment. On the day of the experiment, mice were euthanized using an overdose of ketamine (Ketavet; Zoetis, USA) and xylazine (Rompun; Bayer, Germany). After cervical dislocation, animals were briefly perfused transcardially with a freshly-made ice-cold carbogen-bubbled NMDG-HEPES solution containing (mM): 93 NMDG, 2.5 KCl, 1.2 NaH_2PO_4, 5 L(+)ascorbic acid, 2 thiourea, 3 sodium pyruvate, 10 $MgSO_4$, 0.5 $CaCl_2$, 20 HEPES, 30 $NaHCO_3$, 25 glucose and 10 N-acetyl-L-cysteine, titrated to pH 7.3 with HCl (*73*). After dissection, brains were sliced at 300 μm thickness in chilled carbogen-bubbled NMDG-HEPES solution using a vibration microtome (HM 650V; Themo Scientific, USA). Three coronal slices covering the POA region

(approximately at Bregma AP: +0.24 to -0.16 mm) were recovered per brain. Thereafter, brain slices were allowed to recover for 15 min in carbogen-bubbled NMDG-HEPES solution at 32 °C. Afterwards, tissue slices were transferred to a chamber at room temperature filled with carbogen-bubbled ACSF containing (mM): 125 NaCl, 2.5 KCl, 25 $NaHCO_3$, 1.25 NaH_2PO_4, 1 $MgCl_2$, 2 $CaCl_2$ and 25 glucose until used for imaging within a period of four hours.

For GCaMP6 calcium-imaging, experiments were performed using an upright microscope (BX51W; Olympus, Japan) attached to a motorized base plate (SliceScope SS-1000-00; Scientifica, UK), a 20X objective (XLUMPLFLN 20XW Plan Fluorit; Olympus, Japan), 470 nm excitation illumination (pE-2; CoolLED, UK) and a digital CCD camera (ORCA-R2 C10600-10B; Hamamatsu, Japan). Camera frequency acquisition was set typically at 10 Hz. During experiments, slices were continually perfused with ACSF, gassed with 95% O_2 and 5% CO_2 at 3 ml/min and bath temperature was monitored using a thermistor (TA-29; Warner Instrument, USA). Changes in bath temperature were performed and recorded using an in-line temperature controller (CL-200; Warner Instruments, USA) commanded externally using an A/D board (Digidata 1440A; Molecular Devices, USA) and pClamp10.3 software (Molecular Devices, USA).

Image acquisition and regions of interest (ROI) analysis were performed using MetaFluor 7.1 (Molecular devices, USA). Specifically, ROIs were placed over the cell bodies to record somatic calcium responses (*74*). The fluorescence time course of each cell was measured by averaging all pixels within the ROI to estimate the relative calcium responses $=\Delta F/F0=(F_i-F_{bgi})-F0/F0$, where F_{bgi} was the mean fluorescence of a background ROI placed at the darkest region of the field of view at time i and F0 was calculated as

the mean fluorescence of the 10 lowest values during the first 100 seconds of imaging. The heat stimulation was performed by increasing bath temperature three times every 5 minutes from the baseline temperature (33±1 °C) to 38±1 °C for two minutes. After the temperature protocol was applied, slices were perfused with room-temperature high potassium ACSF solution (HiK), with composition similar to the aforementioned ACSF solution but containing KCl 40 mM (osmolarity was preserved by reducing NaCl concentration to 85 mM). Only cells that did respond to the HiK stimulation were further analyzed.

The relative heat response of each cell was calculated as the maximum amplitude of the calcium signal during the first heat stimulation (Fig 2B). The warm response was calculated as the amplitude of the peak of the calcium response during the first stimulation relative to the amplitude of the peak of the calcium response during HiK stimulation (fig. S2). For this experiment, 79 and 78 cells from *Nestin-Cre*; *Trpm2-WT* and *Nestin-Cre*; *Tprm2*$^{-/-}$ mice, respectively (three slices per mouse, and two animals per genotype) were analyzed.

There were no significant differences within each genetically-defined (*Trpm2-WT* or *Tprm2*$^{-/-}$*)* group, either when calculating the relative warm responses (mean relative warm response±SEM: *Nestin-Cre*; *Trpm2-WT*(mouse #1)=0.305±0.043, N=45; *Nestin-Cre*; *Trpm2-WT*(mouse #2)=0.389±0.072, N=34, P=0.3571; *Nestin-Cre*; *Trpm2*$^{-/-}$(mouse #1)=0.112±0.041, N=47; *Nestin-Cre*; *Trpm2*$^{-/-}$*(*mouse #2)=0.110±0.058, N=31, P=0.7132; two-tailed Mann-Whitney test) or when calculating normalized warm responses (mean normalized warm response±SEM: *Nestin-Cre*; *Trpm2-WT*(mouse #1)=0.152±0.0.021, N=45; *Nestin-Cre*; *Trpm2-WT*(mouse #2)=0.180±0.041, N=34,

P=0.6311; *Nestin-Cre*; *Tprm2*$^{-/-}$*(*mouse #1)=0.028±0.014, N=47; *Nestin-Cre; Tprm2*$^{-/-}$ *(*mouse #2)=0.029±0.073 7, N=31, P=0.9674; two-tailed Mann Whitney test). The only significant difference was detected when comparing warm responses of neurons from *Trpm2-WT* and *Tprm2*$^{-/-}$ mice (mean relative calcium responses upon heat stimuli ± SEM: *Nestin-Cre; Trpm2*$^{-/-}$: 0.111±0.033, N=78, *Nestin-Cre; Trpm2-WT*: 0.341±0.040, N=79, P<0.0001, two-tailed Mann-Whitney test).

3. PGE_2, IL-1β and IL-6 microinjections and telemetric T_{core} measurement

3.1 Cannula and telemetry transmitter implantation

Trpm2$^{+/+}$ and *Trpm2*$^{-/-}$ littermate adult (3-4 month old) mice of both genders were used in these experiments. General surgical procedures were performed as mentioned in section 3.1. A small hole on the skull was drilled at coordinate Bregma: ML 0.30 mm, AP 0.00 mm. A 5 mm long guide cannula (0.46 mm OD and 0.24 mm ID) was implanted (model C315GRL/Spc; Plastic One, USA) and secured using dental cement (Cyano Veneer; Hager & Werken, Germany). Right after implantation, a dummy cannula of 5 mm in length was screwed onto the guide cannula to prevent contaminants from entering the brain (model C315DC/Spc; Plastic One, USA). A sterile telemetric temperature transmitter (TA11TA-F10; Data Sciences International, USA) was implanted in the abdominal cavity. Then muscle and skin layers were separately sutured with absorbable surgical threads (Marlin®; Catgut, Germany).

3.2 Core body temperature measurement by telemetry

Mice were allowed to recovery for at least one week after temperature transmitter implantation into the body cavity and cannula implantation in the POA. The circadian temperature cycle was used to assess whether animals had recovered from surgery. For the PGE_2-induce fever models, 2 µl of a solution containing 0.2 nmol/µl PGE_2 or 2 nmol/µl PGE_2 (P6532; Sigma, USA) or vehicle (50% DMSO in saline) were injected into the POA at 1 µl/min using an injection cannula of 6 mm below pedestal (model C315I/Spc; Plastic One, USA) and an automatic microinjector (UMP3 with SYS-micro4 controller; WPI, USA) under isofluran anesthesia (isofluran 1.5%, N_2O 70% and O_2 30%). For the interleukin-induced fever models, 2 µl of a solution containing 10 ng/µl IL-1β or a mixture containing 50 ng/µl IL-1β and 100 ng/µl IL-6 nmol/µl (SRP8033 and SRP3330 respectively; Sigma, USA) or vehicle (saline) were injected into the POA at 1 µl/min in restrained animals using the above-mentioned cannula model and microinjector. The pyrogen-induced fever was monitored at 22°C ambient temperature for the PGE_2 experiments and at 30°C for the interleukin experiments.

The injection sites were verified *postmortem* subsequent to injection of 1µl of a solution of 1 mg/ml alcian blue (A5268; Sigma, USA) through the injection cannula and by tracking the scar left by the guide cannula on the tissue. For maximal body temperature analysis, the highest three T_{core} values reached by each mouse during febrile response were averaged and the mean value was used to calculate maximal T_{core} per mouse.

For time-course analysis of the low-dose (0.4 nmol) PGE_2-induced fever responses, due to the skipped/missing telemetric data points (18 missing values), non-repeated measures (non-RM) two-way ANOVA was chosen to analyze the febrile responses. T_{core} in PGE_2-

injected groups (N=5 and 4 mice for *TrpM2*$^{+/+}$ and *TrpM2*$^{-/-}$, respectively) was independent of genotype (F(1,122)=1.353, P>0.05, non-RM two-way ANOVA).

For time-course analysis of the high-dose (4 nmol) PGE_2-induced fever responses, due to the skipped/missing telemetric data points (11 missing values in total for both, vehicle and PGE_2-injected groups), non-repeated measures (non-RM) two-way ANOVA followed by Fisher´s LSD *post hoc* test was applied. T_{core} in PGE_2-injected groups (N=10 and 9 mice for *TrpM2*$^{+/+}$ and *TrpM2*$^{-/-}$, respectively) was dependent on genotype (F(1,318)=40.78, P<0.0001, non-RM two-way ANOVA) and time (F(18,318)=52.51, P<0.0001, non-RM two-way ANOVA). T_{core} in vehicle-injected groups was not dependent on genotype (F(1,316)=1.16, P=0.2824, non-RM two-way ANOVA) but it was dependent on time (F(18,316)=19.67, P<0.0001, non-RM two-way ANOVA). Interaction between factors (time and genotype) was detected neither in PGE_2-injected nor vehicle-injected groups (P(interaction) in PGE_2-injected groups=0.9271 and P(interaction) in vehicle-injected groups=0.9973, non-repeated measures two-way ANOVA).

For time-course analysis of the IL-1β-induced fever responses, because of the skipped/missing telemetric data points (8 missing values), non-repeated measures (non-RM) two-way ANOVA followed by Fisher´s LSD *post hoc* test was applied. T_{core} in IL-1β-injected groups (N=5 mice for *TrpM2*$^{+/+}$ and *TrpM2*$^{-/-}$, respectively) was dependent on genotype (F(1,736)=38.40, P<0.0001, non-RM two-way ANOVA) and time (F(92,736)=5.63, P<0.0001, non-RM two-way ANOVA). Interaction between factors (time and genotype) was not detected (P(interaction)=0.15, P>0.05, non-repeated measures two-way ANOVA). However, *post-hoc* Fisher´s LSD test showed no significant differences between any informative paired-comparisons.

For time-course analysis of the IL-1β and IL-6 combination-induced fever responses, due to the skipped/missing telemetric data points (2 missing values, non-repeated measures (non-RM) two-way ANOVA followed by Fisher´s LSD *post hoc* test was applied. T_{core} in IL-1β and IL-6-coinjected groups (N=4 and 5 mice for *TrpM2*$^{+/+}$ and *TrpM2*$^{-/-}$, respectively) was dependent on genotype ($F(1,677)=195.2$, $P<0.0001$, non-RM two-way ANOVA) and time ($F(96,677)=3.60$, $P<0.0001$, non-RM two-way ANOVA). Interaction between factors (time and genotype) was detected ($P(interaction)=1.291$, $P<0.05$, non-repeated measures two-way ANOVA).

4. DREADD viral infection and telemetric measurement

4.1 Stereotactic DREADD viral infection and telemetric implantation

The stereotactic injections of viral particles followed the same procedure as detailed in section 3.1. 8-week-old mice were bilaterally injected with AAV particles into the POA (serotype 8, 120nl, coordinates, Bregma: AP:0.800 mm, DV:−5.000 mm, M L: ±0.500 mm). Gq-DREADD (AAV8-DIO-hM3Dq-mCherry), Gi-DREADD (AAV8-DIO-hM4Di-mCherry) and cherry control (AAV8-DIO-mCherry) virus were all purchased from Vector Core (University of North Carolina). Telemetric transmitters were implanted according to section 3.1.

The animals were allowed to recover for two weeks before telemetric measurements. The circadian temperature cycle was used to assess whether animals had recovered from surgery and viral injections. All stereotactic injection sites were verified by immunohistochemistry (see section 6.4. below).

4.2 Telemetric measurement

Similar to section 3.2, animals were housed in the home cage for telemetric recordings. *Trpm2-Cre* (N=12), *Vglut2-Cre* (N=4) and *Vgat-Cre* (N=3) mice were handled daily for one week before the experiment to habituate the animals. On day 1, day 3 and day 5, mice were injected with saline (i.p.) at 9:00 am. On day 2, day 4 and day 6, 0.3 mg/kg CNO (BML-NS105-0025, Enzo, diluted in saline) was administered (i.p.) at 9:00 am. Equivalent volumes of saline or CNO solution were delivered.

T_{core} was measured telemetrically as described in 3.2. Saline and CNO responses were averaged over three trials per animal. The relative change of T_{core} compared to the baseline was calculated and plotted (ΔT_{core}).

In *Trpm2-Cre* DREADD experiments, repeated-measures two-way ANOVA detected no significant differences between saline-treated Gq-DREADD, Gi-DREADD and Cherry virus-infected animals ($F(2,9)=0.86$, $P=0.45$). Similarly, the same test found no significant difference of the treatment (saline vs. CNO) in Cherry control virus-infected animals ($F(1,6)=1.55$, $P=0.26$). However, a significant effect of treatment (saline v.s CNO) in both Gq-DREAADD and Gi-DREADD virus-infected animals was detected by repeated-measures two-way ANOVA testing ($F(1,6)=75.64$, $P=0.0001$ and $F(1,6)=38.6$, $P=0.0008$, respectively).

In *Vglut2-Cre* experiments, repeated-measures two-way ANOVA detected significant differences between saline- and CNO-treated Gq-DREADD infected animals ($F(1,6)=86.08$, $P<0.0001$). In *Vgat-Cre* experiments, repeated-measures two-way ANOVA detected no significant differences between saline- and CNO-treated Gq-DREADD virus-infected animals ($F(1,4)=0.44$, $P=0.55$).

When comparing Gq-DREADD infected *Trpm2-Cre*, *Vglut2-Cre* and *Vgat-Cre* animals, repeated-measures two-way ANOVA detected no significant differences when animals were treated with saline ($F(2, 8)=2.27$, $P=0.17$), suggesting that the genetic background of the animals does not significantly contribute to the overall ΔT_{core} changes. However, by applying the same test upon CNO-treatment, significant differences were discovered ($F(2, 8)=27.49$, $P=0.0003$). Subsequently, the *post hoc* Fisher's LSD test detected a significant difference between CNO-treated *Trpm2-Cre* and *Vgat-Cre* ($P=0.0003$), but no difference between CNO-treated *Trpm2-Cre* and *Vglut2-Cre* animals ($P=0.40$). Therefore, we concluded that the extent of CNO-induced hypothermia reached a comparable extent in Gq-DREADD infected *Trpm2-Cre* and *Vglut-Cre* animals.

4.3 Infrared imaging

Mice were imaged in their home cages with a highly sensitive infrared camera (VarioCAM; InfraTec, Germany) positioned 25 cm above the cage floor. Thermograms were collected at 1 Hz and analyzed by IRBIS 3 software (InfraTec). In brief, the tails were outlined manually on individual images and the average surface temperatures ($T_{surface}$) of three images were calculated for any given time point. For each animal and time point after CNO/saline treatment, the relative change of temperature ($\Delta T_{surface}$) is calculated by $T_{surface}$ minus the baseline $T_{surface}$ at time point 0 min.

Repeated two-way ANOVA measures detected significant difference between Gq-DREADD and Cherry control virus infected mice (N=4, per viral type) upon CNO treatment ($F(1, 5)=9.3$ $P=0.03$). *Post hoc* Fisher's LSD test was applied to compare differences between each time point. Using this test, the difference was found to be

borderline non-significant between Gi-DREADD and Cherry control virus infected mice upon CNO treatment ($F(1,4)=5.2$, $P=0.085$).

5. Histology

5.1 Immunocytochemistry

Mice were transcardially perfused with 10 ml PBS followed by 40 ml 4% PFA. Brains were dissected out and postfixed overnight in 4% PFA at 4 °C with gentle agitation. After several washes with PBS 50 µm vibratome brain sections were collected into 24-well plates. Floating sections were blocked with 1% goat serum in PBS containing 0.3% TritonX-100 (PBX0.3) for at least 1 h. Sections were then incubated with rabbit anti Trpm2 (1:1000) (*10*) and mouse anti NFM (to label fiber tracts used as landmarks, 1:100; 2H3, DSHB) diluted in blocking solution overnight and washed extensively with PBX0.3. Sections were then incubated with secondary antibodies (HRP anti rabbit 1:2000, Alexa488 anti mouse 1:1000) for a minimum of 3 hours and washed with PBX0.3, PBS and PBS/10 mM imidazole. Tyramid signal amplification (TSA) was used for *Trpm2* visualization using self-made rhodamine tyramide (*75*) in PBS containing 10 mM imidazole and 0.001% H_2O_2 for 30 min at room temperature. Sections were washed extensively with PBS containing 0.1% Tween-20 and mounted using Immu-Mount (Shandon).

5.2 *In situ* hybridization

For *in situ* hybridizations we used either 20 µm cryo-sections or 50 µm free-floating vibratome sections. For cryo-sections brains were freshly dissected, directly embedded into OCT and frozen on dry ice/ethanol bath. 20 µm cryo-sections were cut on a Leica CM3050S cryostat, dried and stored at -80 °C until use. For floating sections, mice were transcardially perfused with 10 ml PBS followed by 40 ml 4% PFA. Brains were dissected out and postfixed overnight in 4% PFA at 4 °C with gentle agitation. 50 µm vibratome sections were cut on a Leica VT1200S vibratome and collected and stored in 1% PFA at 4 °C until use. DREADD virus infected animals were first i.p. injected with 0.3 mg/kg CNO. Thirty minutes afterwards, the animals were sacrificed for *in situ* staining of *Fos*.

In situ hybridization was performed using standard procedures (*76*). In brief, DIG- and/or FITC-labeled cRNA probes were used for hybridization on either free floating- or cryosections. Hybridization was performed overnight at 65 °C. Sections were washed at 60 °C twice in 2xSSC/50% Formamide/0.1% N-lauroylsarcosine, treated with 20 µg/ml RNAse A for 15 min at 37 °C, washed twice in 2xSSC/0.1% N-lauroylsarcosine at 37 °C for 20 min and twice in 0.2xSSC/0.1% N-lauroylsarcosine at 37 °C for 20 min. Sections were blocked in MABT/10% goat serum/1% Blocking reagent (Roche, cat# 11096176001). For NBT/BCIP staining sections were incubated overnight with sheep anti-DIG-AP (1:1000, Roche 11093274910). After washing staining was performed using NBT/BCIP in NTMT until satisfactory intensity. Double fluorescent *in situs* were stained by two consecutive rounds of TSA amplification with intermediate peroxidase inactivation. Sections were incubated with sheep anti-FITC-POD (1:2000, Roche cat#

11426346910) or sheep anti DIG-POD (1:1000, Roche cat# 11207733910) and TSA was performed using biotin-tyramide or rhodamine-tyramide (*15*). Subsequently sections were incubated with Streptavidin-Cy2 and DAPI in blocking solution, washed and mounted in Immu-Mount (Shandon).

Trpm2, Vglut2, tdTomato, Fos, Gad1 and Cre probes covered the ORF of the respective gene. Oxt, Avp, Trh , Crh and Trpm3 probes share identical sequences with the probes used by Allen brain atlas.

5.3 AP staining

Trpm2-Cre;Z/AP animals were transcardially perfused with 10 ml PBS followed by 40 ml 4% PFA. Brains were dissected out and cryo-protected with 30% sucrose/PBS at 4 ^{o}C. Gelatin embedded brains were cut on a Leica SM2010 sliding microtome. 50 μm free-floating sections were first incubated in PBS containing 2 mM Mg^{2+} at 70 ^{o}C for 1 hour to inactivate the endogenous alkaline phosphatase activity. Subsequently the sections were stained with NBT/BCIP in NTMT at room temperature until satisfactory signals intensity has been achieved. Sections were mounted on glass slides in Immu-Mount.

5.4 Immunohistochemistry

DREADD virus-infected animals were transcardially perfused with PBS followed by 4% PFA. Brains were dissected and cryo-protected in PBS containing 30% sucrose at 4 ^{o}C overnight. Gelatin embedded brains were cut on a Leica SM2010 sliding microtome. 40 μm brain sections were mounted on glass slides in Immu-Mount. Virally encoded

mCherry signals were inspected for labeling of the POA. Only correctly targeted animals were included in the study.

5.5 Cell counting

Confocol images of the POA were first manually assigned by area/nuclei according to the Paxinos Atlas. The appropriate brain area was determined based on landmark structures such as the shape and expansion of the ventricles, anterior commissure and optic tract. Labeled cells were counted manually in ImageJ/FIJI.

5.6 Image acquisition and analysis

Fluorescence images were taken on an A1R or C2+ confocal microscope or on a Ni-E wide field microscope, bright field image acquisition was performed on a Ni-E wide field microscope (Nikon imaging center, Heidelberg). Image analysis, conversion and assembly were done using NIS-Elements AR (Nikon), ImageJ/Fiji, Adobe Photoshop and Illustrator. Brain schemes shown in the manuscript (Fig.1D, Fig.3D, Fig.S1A and Fig.S2E) were modified from Paxinos and Franklin, 2001.

6. Data and Statistical analysis

Data was analyzed using Excel (Microsoft Office 2010 for Windows, Microsoft software) and traces from calcium-imaging experiments were analyzed using Clampfit (Ver.10.3; Molecular Devices, USA). Statistical tests were performed using GraphPad 6 (GraphPad Prism 6.0, GraphPad software, USA). Heat-maps showing calcium responses were

generated using the heatmap.2 function of the R package gplots (https://cran.r-project.org/web/packages/gplots/index.html).

Results are presented as mean ± standard error of the mean (SEM) unless indicated otherwise. The non-repeated-measures two-way analysis of variance (ANOVA) was applied to analyze time-course differences in T_{core} between *Trpm2*$^{+/+}$ and *Trpm2*$^{-/-}$ mice, followed by Fisher's LSD *post hoc* testing of individual time points. For telemetric DREADD experiments, statistical significance was evaluated by repeated-measures two-way ANOVA, and Fisher's LSD *post hoc* testing. Two-tailed *t*-test for normally distributed data or two-tailed Mann-Whitney test for non-normally distributed data were used for comparisons. Unpaired tests were used for comparisons between *Trpm2*$^{+/+}$ and *Trpm2*$^{-/-}$ mice and paired tests for evaluating CNO- and saline-treated animals. Distribution of data was assayed using the KS normality test, the D´agostino and Pearson omnibus normality test and the Shapiro-Wilk normality test. '*' signifies $P<0.05$, '**' $P<0.01$, and '***' $P<0.001$.

Supplementary Figures S1-S4

Fig. S1 Characterization of heat responses in POA neuron cultures by calcium-imaging. (A) Schematic depicting a coronal tissue section of the mouse brain. The area dissected for preparation of dispersed POA neuronal cultures is indicated in red. (**B)** Examples of a representative bright field (BF) image and an fluorescent image of primary POA neuron cultures loaded with the intracellular calcium indicator Fura-2 (scale bar, 50 μm). (**C**) Representative pseudocolor image series of POA cultures loaded with Fura-2 and challenged sequentially with a 45 °C stimulus and high potassium (100 mM, HiK) as indicated. Neuronal activation was assessed by ratiometric (F340/F380) calcium-imaging. The color bar (right) indicates relative intracellular calcium levels. (**D, E)** Cultured mouse POA neurons (D) or HEK293 cells (E) were examined for calcium responses (non-normalized Fura-2 ratios, black traces) to repetitive heat stimuli (45°C, red bars) and high potassium (100 mM, HiK, grey bar) in the presence or absence of the extracellular calcium chelator EGTA (2 mM in nominal Ca^{2+}-free Ringer's solution) or 2-APB (30 μM) as indicated. (**F)** Population analysis of heat responses in cultured POA neurons and HEK293 cells (corresponding to data represented in D and E). Shown are relative peak responses (R_t-R_0) of individual cells to the heat stimulus (for details see Table S1). To err on the side of caution, only POA neurons with a peak temperature response ≥ mean + 5SD of the HEK293-cell response were categorized as warm-sensitive neurons (WSNs) as demarcated by the red line. Note that upon a heat stimulus also HEK293 cells showed a subtle increase in the Fura-2 (F340/F380) ratio. This slight increase likely reflects temperature sensitivity of the Fura-2 dye (20) (HEK293: 246 cells, POA: 491 neurons,

POA+EGTA (WSNs only): 88 neurons). Please refer to Table S1 for details. (**G-K**) Cultured mouse POA neurons were examined for calcium responses (black traces) to repetitive heat stimuli (45 °C, red bars) and high potassium (100 mM, HiK, not shown). The effect of the indicated pharmacological agents (grey bars) on warm sensitivity was assessed: (G) Serca-Pump blocker cyclopiazonic acid (CPA, 10 μM); (H) L-type voltage-gated calcium channel blocker nifedipine (Nif, 10 μM); (I) broad-spectrum ion channel blocker ruthenium red (RR, 10 μM); (J, K) voltage-gated sodium channel blocker tetrodotoxin (TTX, 1 μM), note that a partially TTX-sensitive population (J) and a TTX-insensitive population of WSNs (K) could be identified. (**L**) Summary of the results shown in Fig 1A and S1D, and S1G-K expressed as percent heat response compared to control (Ringer's) conditions; Student's *t*-test, $^{**}P<0.01$. (**M**) Schematic depicting overlap of 2-APB-sensitive and thermosensitive ion channels. (**N**) Cultured POA neurons (red trace) or sensory dorsal root ganglion neurons (DRG, black trace) were sequentially challenged with the TRPM3 agonist pregnenolone sulfate (PS, 10 μM), capsaicin (Cap, 1 μM) and high potassium (HiK, 100 mM) as indicated and responses assessed by calcium-imaging. Note that neither PS nor Cap was able to elicit any response in POA neurons under these conditions, but only triggered calcium responses in control DRG cultures. (**O**) *In situ* hybridization of a coronal brain section from an adult mouse at the level of the POA, showing pronounced expression of *Trpm3* transcripts in the lateral septal nucleus and more subtle expression in the POA (scale bar, 1 mm). (**P-S**) Electrophysiological whole-cell recordings in voltage clamp mode of adenosine diphosphate ribose- (ADPR-) induced currents in POA neurons identified as WSNs by preceding calcium imaging that was performed before patch-clamping. **(P)** Dialysis of 100 μM ADPR induced a rapidly

evolving inward current at a holding potential of -65 mV. No such current was observed in the absence of ADPR. The ADPR-induced current was partially reduced when extracellular sodium ions (Na^+-free; current reduction 49±8%, n=5, SEM) or extracellular sodium and calcium ions (Na^+-, Ca^{2+}-free) were excluded from the extracellular solution and replaced with N-Methyl-D-Glucamine (NMDG). The remaining current under these NMDG-replacement conditions is likely carried by extracellular potassium ions that are able to pass through the pore of the non-selective cationic TRPM2 ion channel. **(Q)** Current-Voltage (I-V) curves of voltage-clamped WSNs. Shown are recordings of the same cells as in Fig. 1F but at earlier time points after dialysis of the cell with ADPR (grey) and of a cell without ADPR (shades of blue). Note that on average between 1-3 minutes after ADPR exposure, WSNs started to develop a small current that over the next few minutes fully developed into a large current with a characteristic linear current-voltage relation as shown in (R) and Fig. 1F. No such currents were observed in the absence of ADPR. **(R)** Current-Voltage (I-V) curves of individual POA WSNs responding to ADPR (blue). 4 out of 16 WSNs failed to respond to ADPR over the course of a 10-minute recording period (grey). **(S)** Left panel: Average ADPR-induced current density of all 16 analyzed WSNs shown in (R) and compared to the average current density recorded for WSNs in the absence (-) of ADPR (n=9). Current densities were determined at -40 mV for comparison with other cell types expressing TRPM2, see for example (*40*). Right panel: Conductance (i.e. linear slope) of respective I-V curves. All ADPR responding cells have linear I-V curves. Bar plots are mean + SEM. Two-tailed Mann-Whitney test, $^{**}P<0.01$, $^{***}P<0.001$.

Fig. S2 TRPM2 meditates responses to high physiological temperatures and fever but is not required for normothermia in mice. (A) Cultured mouse POA neurons were examined for calcium responses (black trace) to thermal stimuli of increasing magnitude (red trace). Robust 2-APB-sensitive (black bar, 30 μM) calcium responses of dispersed POA neurons were observed at 45.5±0.5 °C. (**B, C)** Population analysis of cellular responses to a temperature stimulus of up to 40 °C recorded in acute POA slices, similar to the analysis shown in Fig. 2C but normalized to high potassium responses (B) and population analysis of high potassium (HiK) responses (C) demonstrate a reduction of the normalized warm responses in acute slices from *Nestin-Cre*; *Trpm2*$^{-/-}$ (mean normalized heat responses±SEM: *Nestin-Cre; Trpm2*$^{-/-}$: 0.028±0.030, N=78; *Nestin-Cre; Trpm2-WT* : 0.164±0.021, N=79, two-tailed Mann-Whitney test, P<0.0001) but no alteration of general excitability when compared to wild type controls (mean calcium response during HiK stimulation±SEM: *Nestin-Cre; Trpm2*$^{-/-}$: 1.981±0.158, N=78, *Nestin-Cre; Trpm2-WT*: 2.001±0.112, N=79, two-tailed Mann-Whitney test, P=0.36). (**D**) Cartoon depicting stereotactic injection into the POA (left panel). Injection of Alcian Blue was used to retrospectively ascertain correct positioning of the injection needle (right panel), subsequent to PGE_2 application and fever measurements shown in Fig. 2E. Scale bar 1 mm. (**E)** Telemetric T_{core} measurements show no difference in diurnal body temperatures between *Trpm2*$^{-/-}$ and *Trpm2*$^{+/+}$ mice, indicating that TRPM2 is not required for maintaining normothermia at basal ambient temperatures. **(F)** Fever induced by injection of a low dose of PGE_2 (0.4 nmol/mouse) into the POA of *Trpm2*$^{-/-}$ mice (black trace) compared to littermate *Trpm2*$^{+/+}$ controls (red trace); N=4 and 5 mice per group, respectively; no significant differences were detected between the fever curves of *Trpm2*$^{-}$

$^{/-}$ and *Trpm2*$^{+/+}$ mice (two way ANOVA F(1,122)=1.353, P>0.05). Mice were briefly anaesthetized before microinjection of PGE_2, resulting in a transient drop of T_{core} at all conditions and genotypes. **(G)** Fever induced by injection of Interleukin 1β (IL-1β, 20 ng) into the POA of *Trpm2*$^{-/-}$ mice (black trace) compared to littermate *Trpm2*$^{+/+}$ controls (red trace); N=5 mice per group per genotype; no significant differences were detected between the fever curves of *Trpm2*$^{-/-}$ and *Trpm2*$^{+/+}$ mice (two way ANOVA F(1,736)=38.40, P<0.0001 followed by *post hoc* Fisher's LSD test, P>0.05). Mice were restrained but not anaesthetized for interleukin injections. **(H)** Fever induced by co-injection of Interleukin 1β (IL-1β, 100 ng) and Interleukin 6 (IL-6, 200 ng) into the POA of *Trpm2*$^{-/-}$ mice (black trace) compared to littermate *Trpm2*$^{+/+}$ controls (red trace); N=5 and 4 mice per group, respectively. Trpm2$^{-/-}$ mice showed a significantly higher fever response compared to Trpm2$^{+/+}$ littermate controls at the indicated time pints (two way ANOVA F(1,677)=195.2, P<0.0001, followed by *post hoc* Fisher's LSD test, *P<0.05). Mice were restrained but not anaesthetized for co-injections. (I) Maximum body temperatures reached during the fever experiments shown in Fig. 2E and fig. S2F-H. Two-tailed unpaired Student's *t*-test for PGE_2 4 nmol condition and two-tailed Mann-Whitney test for all additional conditions. *P<0.05, **P<0.01.

Fig. S3 Generation and characterization of *Trpm2-Cre* mice

(A) Mice expressing iCre recombinase under the control of the endogenous *Trpm2* promotor were generated by inserting a cassette encoding a cleavable 2A peptide followed by iCre, before the *Trpm2* stop codon. The wild type allele, the targeting construct, and the targeted allele are shown as well as the final recombined allele that

results after removing the neomycin selection cassette by crossing the animals with the Flpe expressing deleter strain. Restriction sites and the positions of 3'/5' DNA probes are indicated that were used for screening targeted ES cells by Southern blotting (middle panel) as well as primers (P1 and P2) used for PCR genotyping of *Trpm2-Cre* mice (right panel). (**B**) Immunohistochemistry using antibodies against TRPM2 (cyan) and neurofilament (NFM, magenta) were used to label mouse brain sections covering the POA at different rostral to caudal (r ➔ c) levels. (**C-D**) *In situ* hybridization of brain sections from wild type (B) or *Trpm2-Cre* (C) mice with probes detecting *Trpm2* or *iCre* messages, respectively. Note that both probes robustly label the POA and a weaker signal can also be detected in the cortex, a region that is not labeled by the TRPM2 antibody (B). (**E)**, Alkaline phosphatase staining of brain sections from *Trpm2-Cre* mice crossed with *Z/AP* reporter mice recapitulates the strong labeling of the POA similar to antibody labeling and *in situ* hybridization (B-D) and shows a somewhat patchy pattern in the cortex, likely reflecting lower expression of iCre in this brain region. Scale bar, 1 mm. (**F**) Representative two-color *in situ* hybridizations of a brain section covering the POA from *Trpm2-Cre* mice crossed to a reporter expressing *tdTomato* upon Cre recombination (*Trpm2-Cre*; *Ai9*). *In situ* probes detecting *tdTomato* (red) and *Trpm2* (green) were used. Note that there is essentially complete cellular overlap of the respective preoptic expression pattern. Scale bars, 100 μm. (**G**) Acute POA slice preparations of *Trpm2-Cre* mice co-expressing the calcium indicator GCaMP6 and either Gq-DREADD (left panel) or Gi-DREADD (right panel) were challenged with clozapine-N-oxide (CNO, 0.5 μM and 5 μM respectively) and a high potassium stimulus (HiK, 40 mM) as indicated. Neuronal activity was recorded by GCaMP6-mediated calcium imaging at a constant bath

temperature of 33 °C. Cre-inducible expression cassettes for GCaMP6 and the respective DREADDs were virally introduced by microinjection into the mouse POA two weeks prior to slice preparation. A non-linear pseudo-color scale indicates relative calcium responses. (**H**) Telemetric T_{core} measurements show normal diurnal body temperature regulation in T*rpm2-Cre* mice in the presence or absence of virally encoded Gq-DREADD in POA neurons, indicating that DREADD expression *per se* (and in the absence of the agonist CNO) does not perturb thermoregulation. (**I**) T_{core} was measured telemetrically in *Trpm2-Cre* mice expressing either Gq-DREADD, Gi-DREADD or Cherry control and challenged with CNO (0.3 mg/kg) or vehicle (saline) as indicated and T_{core} curves were recorded as shown in Fig. 3 C, D and H. The area under the curve (AUC - integration of the T_{core} temperature curves over time) is plotted for the indicated conditions. Time interval used for integrations: t=0 min to 2 hour after CNO application; N=4 for each group, two-tailed paired-test. Gq-CNO vs Gq-saline, **P<0.01, Gi-CNO vs. Gi-saline, **P<0.01. Cherry-CNO vs Cherry-saline P=0.12. (**J, K**) Quantification of whole body (J) and interscapular BAT (K) surface temperature difference (ΔT) compared to a time point (t=0 min) before CNO injection. Shown are average surface temperature changes of Gq-DREADD (red), control (black) or Gi-DREADD (green) infected *Trpm2-Cre* mice upon CNO treatment. N=4 mice per group, two way ANOVA followed by *post hoc* Fisher's Least Significant difference (LSD) test. IR imaging of body: Gq-DREADD F(1,6)=13.54, P=0.0103. Gi-DREADD F (1,6)=0.116, P=0.74. IR imaging of BAT: Gq-DREADD F(1,6)=9.3, P=0.003. Gi-DREADD F (1,6)=0.18, P=0.68.

Fig. S4 Activation of PVH-projecting Vglut2$^+$ but not Vgat$^+$ POA neurons recapitulate Trpm2$^+$-driven hypothermia

(A) Illustration depicting the fraction of all preoptic inhibitory (Gad1$^+$, red) and all preoptic excitatory (Vglut2$^+$, blue) neurons that are Trpm2 positive (shades of green). Note that in *Vglut2-Cre* mice only a small fraction (~20%) of Vglut2$^+$ POA neurons are expressing Cre recombinase (shown in D, below). (**B and C)** Representative brain slices demonstrating targeting of the virally encoded, Cre-dependent Gq-DREADD-cherry fusion proteins in the POA of *Vglut2-Cre* (B) and *Vgat-Cre* (C) mice used in experiments shown in Fig. 4B-D and visualized *post hoc* by fluorescent microscopy. Scale bars, 1 mm. (**D**) Representative images of a brain section covering the POA of *Vglut2-Cre* mice and visualizing transcripts for *Cre* recombinase (green) and native *Vglut2* (red) by dual-color *in situ* hybridization. Note that Vglut2-Cre$^+$ neurons only represent a small fraction (~20%) of all Vglut2$^+$ neurons as illustrated in (A). Scale bars, 100 μm. (**E**) *In situ* hybridizations of brain sections from *Trpm2-Cre* and *Vglut2-Cre* mice using a probe to detect *Fos* (green). Two weeks prior to preparation of tissue sections, the mice were either injected or not injected with Cre-dependent viral Gq-DREADD expression constructs as indicated. Thirty minutes before preparation of the tissue sections, all animals were injected with the DREADD agonist CNO. *Fos* labeling revealed Gq-DREADD-dependent neuronal activation in the paraventricular nucleus of the hypothalamus (PVH). Scale bars: 1 mm for main graphs and 200 μm for insets. **(F)** Depicted are two-color *in situ* hybridizations of *Vglut2-Cre* mice preoptically expressing Cre-dependent Gq-DREADD receptors and using probes to detect *Fos* (green), *Oxytocin* (*Oxt*, red) and *Vasopressin* (*Avp*, red) as indicated. Animals were sacrificed and brain

sections covering the PVH were prepared 30 min after CNO stimulation. Scale bar, 100 μm.

Table S1

Calcium imaging analysis of warm-sensitive POA neurons

The table displays the raw calcium imaging data (time course experiment of temperature stimulations) of HEK293 cells, and cultured POA neurons of Trpm2$^{+/+}$ and Trpm2$^{-/-}$ mice. Additionally, the "Notes and Statistics" sheet describes the step-by-step analysis of warm-responsive neurons. Table S1 corresponds to Fig. 1G-I and fig. S1F.

Movie S1

Infrared thermal imaging of a *Trpm2-Cre* mouse preoptically expressing Gq-DREADD receptors. Shown is a time-laps movie of a representative Gq-DREADD infected *Trpm2-Cre* mouse at different times before and after CNO injection and imaged with an IR camera from above. The movie is about 1 minute long and covers a total time span of 2 hours in real-time. The movie is broken up into 4 episodes as indicated. Episode 1: before CNO injection; episode 2: 12 to 19 minutes after CNO injection; episode 3: 1 hour after CNO injection; episode 4: 2 hours after CNO injection.

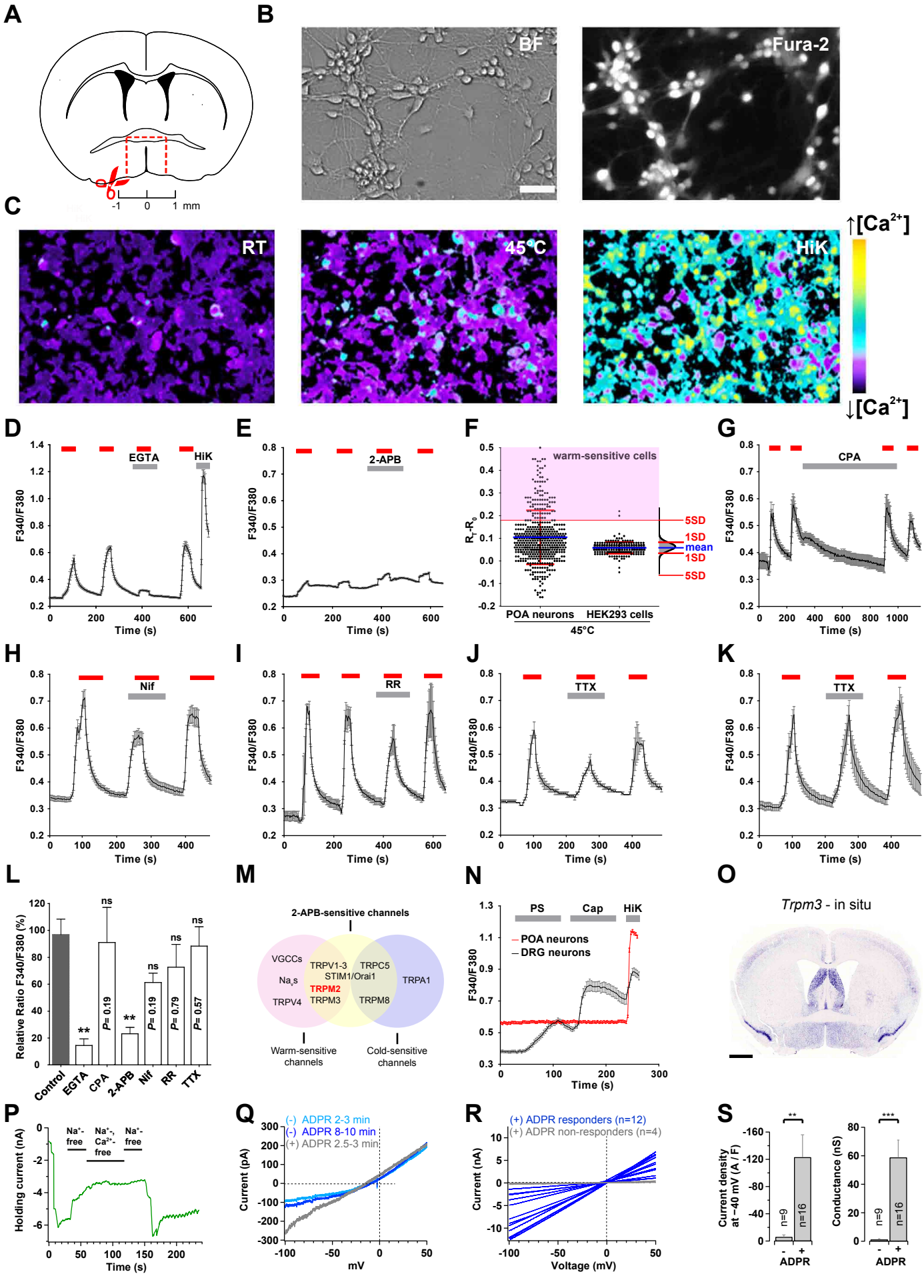
A
B
BF
Fura-2
C
RT
45°C
HiK
↑[Ca2+]
↓[Ca2+]
D
EGTA
HiK
F340/F380
Time (s)
E
2-APB
F340/F380
Time (s)
F
warm-sensitive cells
R-R0
5SD
1SD
mean
1SD
5SD
POA neurons
HEK293 cells
45°C
G
CPA
F340/F380
Time (s)
H
Nif
F340/F380
Time (s)
I
RR
F340/F380
Time (s)
J
TTX
F340/F380
Time (s)
K
TTX
F340/F380
Time (s)
L
Relative Ratio F340/F380 (%)
ns
**
P= 0.19
**
P= 0.19
ns
P= 0.79
ns
P= 0.57
ns
Control
EGTA
CPA
2-APB
Nif
RR
TTX
M
2-APB-sensitive channels
VGCCs
Na+s
TRPV4
TRPV1-3
STIM1/Orai1
TRPM2
TRPM3
TRPC5
TRPM8
TRPA1
Warm-sensitive channels
Cold-sensitive channels
N
PS
Cap
HiK
POA neurons
DRG neurons
F340/F380
Time (s)
O
Trpm3 - in situ
P
Na+-free
Na+-, Ca2+-free
Na+-free
Holding current (nA)
Time (s)
Q
(-) ADPR 2-3 min
(-) ADPR 8-10 min
(+) ADPR 2.5-3 min
Current (pA)
mV
R
(+) ADPR responders (n=12)
(+) ADPR non-responders (n=4)
Current (nA)
Voltage (mV)
S
Current density at −40 mV (A / F)
**
n=9
n=16
ADPR
Conductance (nS)
***
n=9
n=16
ADPR

Fig. S1

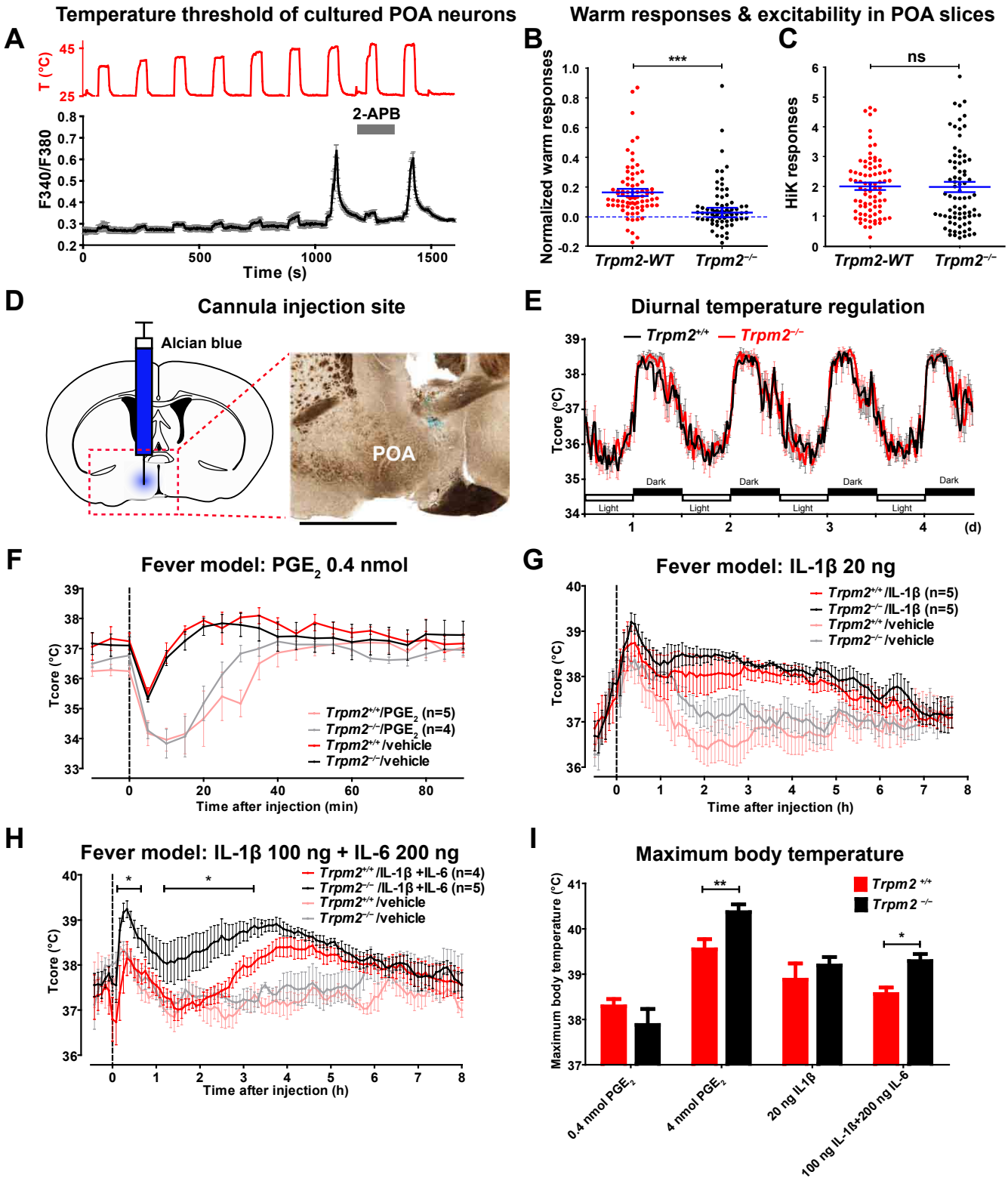
Temperature threshold of cultured POA neurons
A
T (°C)
45
25
2-APB
F340/F380
0.8
0.7
0.6
0.5
0.4
0.3
0.2
0
500
1000
1500
Time (s)
Warm responses & excitability in POA slices
B
***
Normalized warm responses
1.0
0.8
0.6
0.4
0.2
0.0
-0.2
Trpm2-WT
Trpm2−/−
C
ns
HiK responses
6
5
4
3
2
1
0
Trpm2-WT
Trpm2−/−
D
Cannula injection site
Alcian blue
POA
E
Diurnal temperature regulation
Trpm2+/+
Trpm2−/−
Tcore (°C)
39
38
37
36
35
34
Dark
Light
1
2
3
4
(d)
F
Fever model: PGE2 0.4 nmol
Tcore (°C)
39
38
37
36
35
34
33
Trpm2+/+/PGE2 (n=5)
Trpm2−/−/PGE2 (n=4)
Trpm2+/+ /vehicle
Trpm2−/−/vehicle
0
20
40
60
80
Time after injection (min)
G
Fever model: IL-1β 20 ng
Trpm2+/+ /IL-1β (n=5)
Trpm2−/− /IL-1β (n=5)
Trpm2+/+ /vehicle
Trpm2−/− /vehicle
Tcore (°C)
40
39
38
37
36
0
1
2
3
4
5
6
7
8
Time after injection (h)
H
Fever model: IL-1β 100 ng + IL-6 200 ng
Trpm2+/+ /IL-1β +IL-6 (n=4)
Trpm2−/− /IL-1β +IL-6 (n=5)
Trpm2+/+ /vehicle
Trpm2−/− /vehicle
*
*
Tcore (°C)
40
39
38
37
36
0
1
2
3
4
5
6
7
8
Time after injection (h)
I
Maximum body temperature
Trpm2 +/+
Trpm2 −/−
**
*
Maximum body temperature (°C)
41
40
39
38
37
0.4 nmol PGE2
4 nmol PGE2
20 ng IL1β
100 ng IL-1ß+200 ng IL-6

Fig. S2

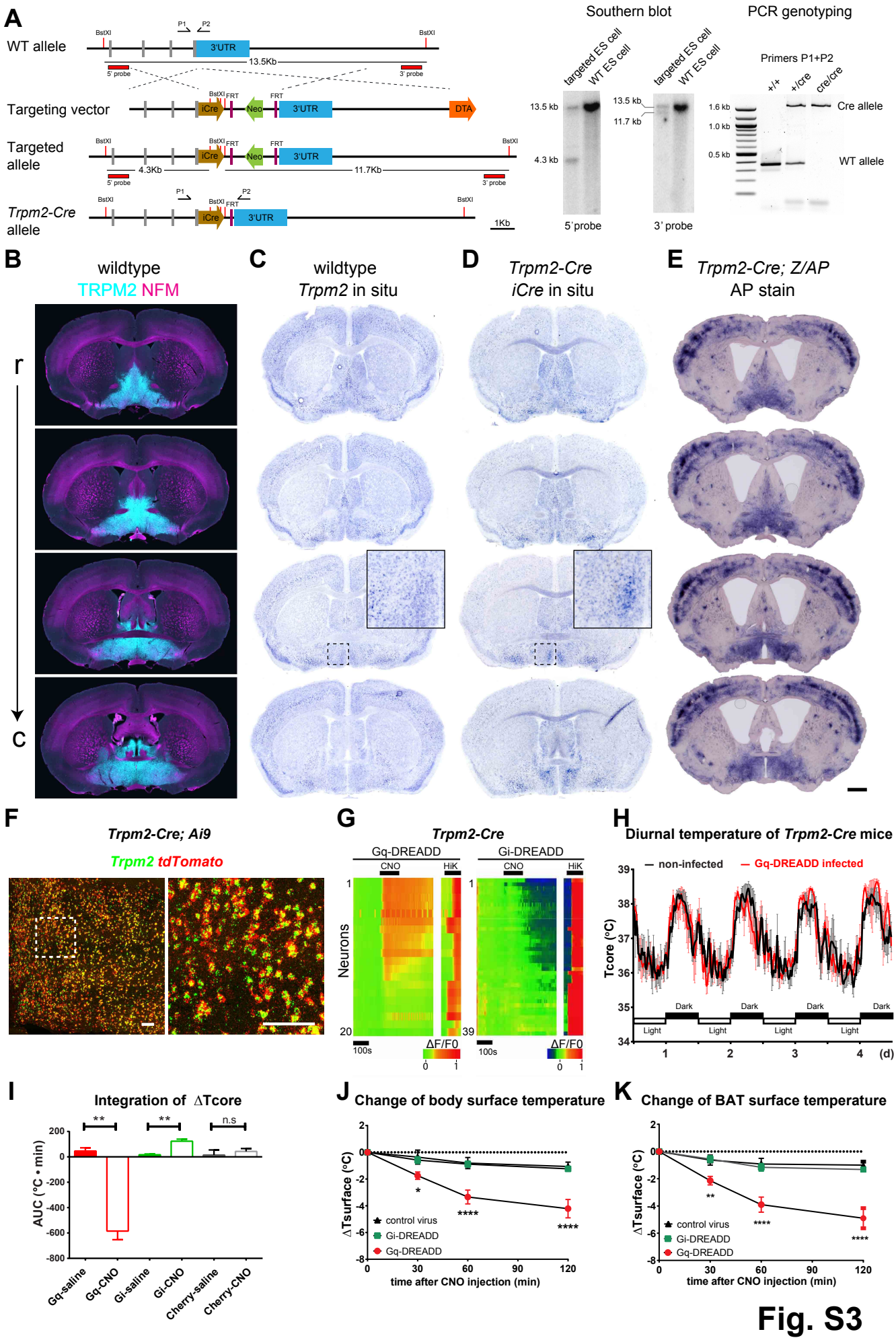
A
WT allele
Targeting vector
Targeted allele
Trpm2-Cre allele
BstXI
P1
P2
3'UTR
13.5Kb
5' probe
3' probe
iCre
Neo
FRT
DTA
4.3Kb
11.7Kb
1Kb
Southern blot
PCR genotyping
targeted ES cell
WT ES cell
13.5 kb
4.3 kb
11.7 kb
5' probe
3' probe
Primers P1+P2
+/+
+/cre
cre/cre
1.6 kb
1.0 kb
0.5 kb
Cre allele
WT allele
B
wildtype
TRPM2 NFM
r
c
C
wildtype
Trpm2 in situ
D
Trpm2-Cre
iCre in situ
E
Trpm2-Cre; Z/AP
AP stain
F
Trpm2-Cre; Ai9
Trpm2 tdTomato
G
Trpm2-Cre
Gq-DREADD
Gi-DREADD
CNO
HiK
Neurons
100s
ΔF/F0
H
Diurnal temperature of Trpm2-Cre mice
non-infected
Gq-DREADD infected
Tcore (°C)
Dark
Light
(d)
I
Integration of ΔTcore
AUC (°C • min)
n.s
Gq-saline
Gq-CNO
Gi-saline
Gi-CNO
Cherry-saline
Cherry-CNO
J
Change of body surface temperature
ΔTsurface (°C)
control virus
Gi-DREADD
Gq-DREADD
time after CNO injection (min)
K
Change of BAT surface temperature
ΔTsurface (°C)
control virus
Gi-DREADD
Gq-DREADD
time after CNO injection (min)

Fig. S3

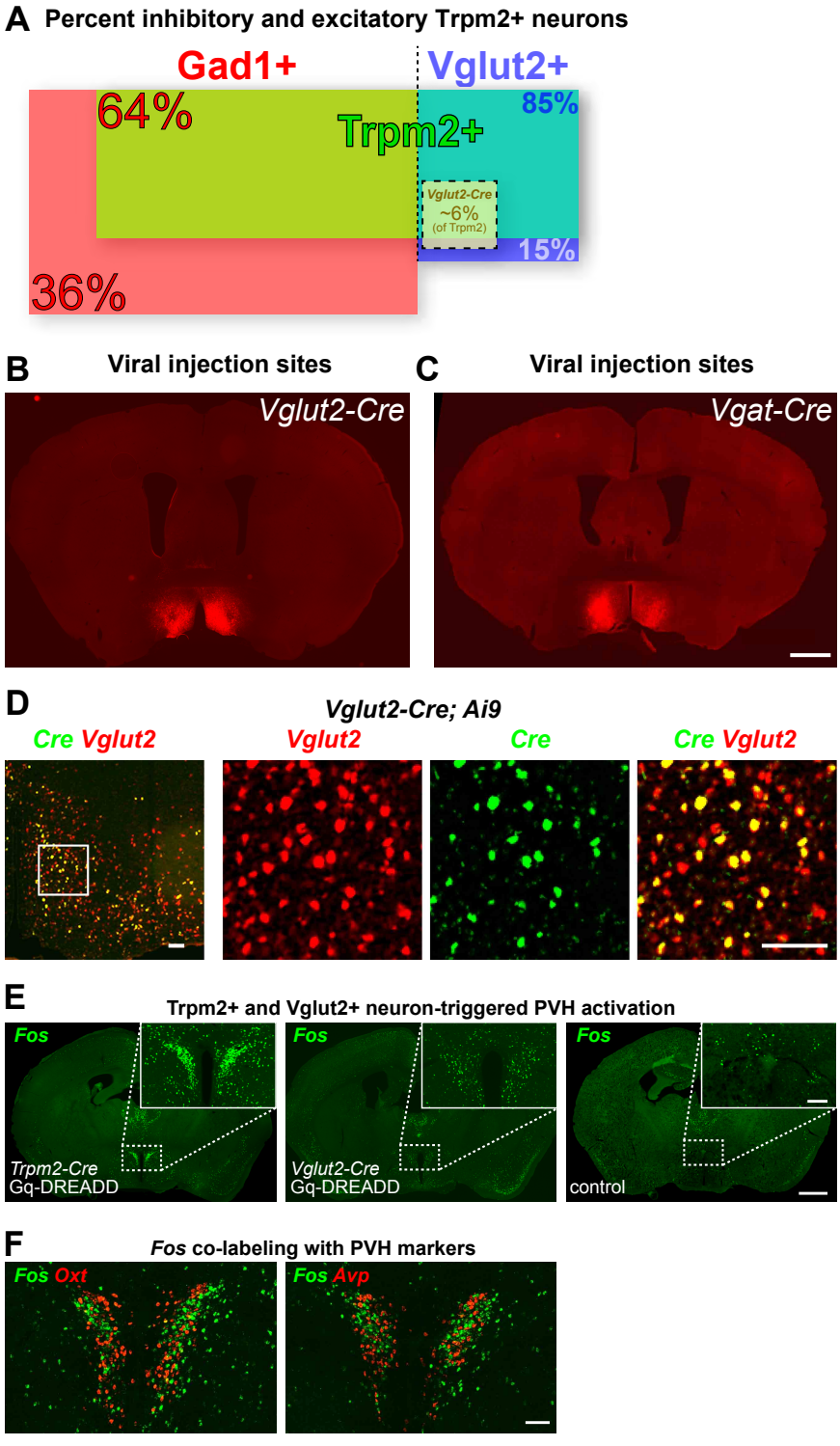
A
Percent inhibitory and excitatory Trpm2+ neurons
Gad1+
Vglut2+
64%
Trpm2+
85%
Vglut2-Cre
~6%
(of Trpm2)
15%
36%
B
Viral injection sites
Vglut2-Cre
C
Viral injection sites
Vgat-Cre
D
Vglut2-Cre; Ai9
Cre Vglut2
Vglut2
Cre
Cre Vglut2
E
Trpm2+ and Vglut2+ neuron-triggered PVH activation
Fos
Trpm2-Cre
Gq-DREADD
Fos
Vglut2-Cre
Gq-DREADD
Fos
control
F
Fos co-labeling with PVH markers
Fos Oxt
Fos Avp

Fig. S4

References and Notes

1. T. Bartfai, B. Conti, Fever. *Sci. World J.* **10**, 490–503 (2010). Medline doi:10.1100/tsw.2010.50

2. C. B. Saper, A. A. Romanovsky, T. E. Scammell, Neural circuitry engaged by prostaglandins during the sickness syndrome. *Nat. Neurosci.* **15**, 1088–1095 (2012). Medline doi:10.1038/nn.3159

3. S. F. Morrison, Central neural control of thermoregulation and brown adipose tissue. *Auton. Neurosci.* **196**, 14–24 (2016). Medline doi:10.1016/j.autneu.2016.02.010

4. M. E. Musselman, S. Saely, Diagnosis and treatment of drug-induced hyperthermia. *Am. J. Health Syst. Pharm.* **70**, 34–42 (2013). Medline doi:10.2146/ajhp110543

5. W. D. Dietrich, H. M. Bramlett, Therapeutic hypothermia and targeted temperature management in traumatic brain injury: Clinical challenges for successful translation. *Brain Res.* **1640**, 94–103 (2016). Medline doi:10.1016/j.brainres.2015.12.034

6. T. C. Wu, J. C. Grotta, Hypothermia for acute ischaemic stroke. *Lancet Neurol.* **12**, 275–284 (2013). Medline doi:10.1016/S1474-4422(13)70013-9

7. T. L. Horvath, N. S. Stachenfeld, S. Diano, A temperature hypothesis of hypothalamus-driven obesity. *Yale J. Biol. Med.* **87**, 149–158 (2014). Medline

8. H. C. Heller, L. I. Crawshaw, H. T. Hammel, The thermostat of vertebrate animals. *Sci. Am.* **239**, 102–110, 112–113 (1978). Medline doi:10.1038/scientificamerican0878-102

9. B. A. Baldwin, D. L. Ingram, Effect of heating and cooling the hypothalamus on behavioral thermoregulation in the pig. *J. Physiol.* **191**, 375–392 (1967). Medline doi:10.1113/jphysiol.1967.sp008256

10. H. T. Hammel, J. D. Hardy, M. M. Fusco, Thermoregulatory responses to hypothalamic cooling in unanesthetized dogs. *Am. J. Physiol.* **198**, 481–486 (1960). Medline

11. H. W. Magoun, F. Harrison, J. R. Brobeck, S. W. Ranson, Activation of heat loss mechanisms by local heating of the brain. *J. Neurophysiol.* **1**, 101–114 (1938).

12. E. Satinoff, Behavioral thermoregulation in response to local cooling of the rat brain. *Am. J. Physiol.* **206**, 1389–1394 (1964). Medline

13. B. Folkow, G. Strom, B. Uvnas, Cutaneous vasodilatation elicited by local heating of the anterior hypothalamus in cats and dogs. *Acta Physiol. Scand.* **17**, 317–326 (1949). Medline doi:10.1111/j.1748-1716.1949.tb00578.x

14. B. Conti, M. Sanchez-Alavez, R. Winsky-Sommerer, M. C. Morale, J. Lucero, S. Brownell, V. Fabre, S. Huitron-Resendiz, S. Henriksen, E. P. Zorrilla, L. de Lecea, T. Bartfai, Transgenic mice with a reduced core body temperature have an increased life span. *Science* **314**, 825–828 (2006). Medline doi:10.1126/science.1132191

15. M. M. Fusco, J. D. Hardy, H. T. Hammel, Interaction of central and peripheral factors in physiological temperature regulation. *Am. J. Physiol.* **200**, 572–580 (1961). Medline

16. H. C. Heller, Hypothalamic thermosensitivity in mammals. *Experientia Suppl.* **32**, 267–276 (1978). Medline doi:10.1007/978-3-0348-5559-4_30

17. J. A. Boulant, Neuronal basis of Hammel's model for set-point thermoregulation. *J. Appl. Physiol.* **100**, 1347–1354 (2006). Medline doi:10.1152/japplphysiol.01064.2005

18. T. Nakayama, J. S. Eisenman, J. D. Hardy, Single unit activity of anterior hypothalamus during local heating. *Science* **134**, 560–561 (1961). Medline doi:10.1126/science.134.3478.560

19. T. Nakayama, H. T. Hammel, J. D. Hardy, J. S. Eisenman, Thermal stimulation of electrical activity of single units of the preoptic region. *Am. J. Physiol.* **204**, 1122–1126 (1963).

20. A. E. Oliver, G. A. Baker, R. D. Fugate, F. Tablin, J. H. Crowe, Effects of temperature on calcium-sensitive fluorescent probes. *Biophys. J.* **78**, 2116–2126 (2000). Medline doi:10.1016/S0006-3495(00)76758-0

21. C. Cai, X. Meng, J. He, H. Wu, F. Zou, Effects of ZD7288 on firing pattern of thermosensitive neurons isolated from hypothalamus. *Neurosci. Lett.* **506**, 336–341 (2012). Medline doi:10.1016/j.neulet.2011.11.041

22. I. V. Tabarean, B. Conti, M. Behrens, H. Korn, T. Bartfai, Electrophysiological properties and thermosensitivity of mouse preoptic and anterior hypothalamic neurons in culture. *Neuroscience* **135**, 433–449 (2005). Medline doi:10.1016/j.neuroscience.2005.06.053

23. J. A. Boulant, J. B. Dean, Temperature receptors in the central nervous system. *Annu. Rev. Physiol.* **48**, 639–654 (1986). Medline doi:10.1146/annurev.ph.48.030186.003231

24. R. Palkar, E. K. Lippoldt, D. D. McKemy, The molecular and cellular basis of thermosensation in mammals. *Curr. Opin. Neurobiol.* **34**, 14–19 (2015). Medline doi:10.1016/j.conb.2015.01.010

25. J. Vriens, B. Nilius, T. Voets, Peripheral thermosensation in mammals. *Nat. Rev. Neurosci.* **15**, 573–589 (2014). Medline doi:10.1038/nrn3784

26. H. Wang, J. Siemens, TRP ion channels in thermosensation, thermoregulation and metabolism. *Temperature* **2**, 178–187 (2015). Medline doi:10.1080/23328940.2015.1040604

27. L. Vay, C. Gu, P. A. McNaughton, The thermo-TRP ion channel family: Properties and therapeutic implications. *Br. J. Pharmacol.* **165**, 787–801 (2012). Medline doi:10.1111/j.1476-5381.2011.01601.x

28. H. Z. Hu, Q. Gu, C. Wang, C. K. Colton, J. Tang, M. Kinoshita-Kawada, L. Y. Lee, J. D. Wood, M. X. Zhu, 2-aminoethoxydiphenyl borate is a common activator of

TRPV1, TRPV2, and TRPV3. *J. Biol. Chem.* **279**, 35741–35748 (2004). Medline doi:10.1074/jbc.M404164200

29. K. Togashi, H. Inada, M. Tominaga, Inhibition of the transient receptor potential cation channel TRPM2 by 2-aminoethoxydiphenyl borate (2-APB). *Br. J. Pharmacol.* **153**, 1324–1330 (2008). Medline doi:10.1038/sj.bjp.0707675

30. S. Z. Xu, F. Zeng, G. Boulay, C. Grimm, C. Harteneck, D. J. Beech, Block of TRPC5 channels by 2-aminoethoxydiphenyl borate: A differential, extracellular and voltage-dependent effect. *Br. J. Pharmacol.* **145**, 405–414 (2005). Medline doi:10.1038/sj.bjp.0706197

31. D. M. Bautista, J. Siemens, J. M. Glazer, P. R. Tsuruda, A. I. Basbaum, C. L. Stucky, S. E. Jordt, D. Julius, The menthol receptor TRPM8 is the principal detector of environmental cold. *Nature* **448**, 204–208 (2007). Medline doi:10.1038/nature05910

32. A. Dhaka, A. N. Murray, J. Mathur, T. J. Earley, M. J. Petrus, A. Patapoutian, TRPM8 is required for cold sensation in mice. *Neuron* **54**, 371–378 (2007). Medline doi:10.1016/j.neuron.2007.02.024

33. K. Zimmermann, J. K. Lennerz, A. Hein, A. S. Link, J. S. Kaczmarek, M. Delling, S. Uysal, J. D. Pfeifer, A. Riccio, D. E. Clapham, Transient receptor potential cation channel, subfamily C, member 5 (TRPC5) is a cold-transducer in the peripheral nervous system. *Proc. Natl. Acad. Sci. U.S.A.* **108**, 18114–18119 (2011). Medline doi:10.1073/pnas.1115387108

34. B. Xiao, B. Coste, J. Mathur, A. Patapoutian, Temperature-dependent STIM1 activation induces Ca^{2+} influx and modulates gene expression. *Nat. Chem. Biol.* **7**, 351–358 (2011). Medline doi:10.1038/nchembio.558

35. J. Siemens, S. Zhou, R. Piskorowski, T. Nikai, E. A. Lumpkin, A. I. Basbaum, D. King, D. Julius, Spider toxins activate the capsaicin receptor to produce inflammatory pain. *Nature* **444**, 208–212 (2006). Medline doi:10.1038/nature05285

36. D. E. Clapham, C. Montell, G. Schultz, D. Julius, International Union of Pharmacology, XLIII. Compendium of voltage-gated ion channels: Transient receptor potential channels. *Pharmacol. Rev.* **55**, 591–596 (2003). Medline doi:10.1124/pr.55.4.6

37. J. Vriens, G. Owsianik, T. Hofmann, S. E. Philipp, J. Stab, X. Chen, M. Benoit, F. Xue, A. Janssens, S. Kerselaers, J. Oberwinkler, R. Vennekens, T. Gudermann, B. Nilius, T. Voets, TRPM3 is a nociceptor channel involved in the detection of noxious heat. *Neuron* **70**, 482–494 (2011). Medline doi:10.1016/j.neuron.2011.02.051

38. M. Kashio, T. Sokabe, K. Shintaku, T. Uematsu, N. Fukuta, N. Kobayashi, Y. Mori, M. Tominaga, Redox signal-mediated sensitization of transient receptor potential melastatin 2 (TRPM2) to temperature affects macrophage functions. *Proc. Natl. Acad. Sci. U.S.A.* **109**, 6745–6750 (2012). Medline doi:10.1073/pnas.1114193109

39. A. L. Perraud, A. Fleig, C. A. Dunn, L. A. Bagley, P. Launay, C. Schmitz, A. J. Stokes, Q. Zhu, M. J. Bessman, R. Penner, J. P. Kinet, A. M. Scharenberg, ADP-ribose gating of the calcium-permeable LTRPC2 channel revealed by Nudix motif homology. *Nature* **411**, 595–599 (2001). Medline doi:10.1038/35079100

40. Y. Sano, K. Inamura, A. Miyake, S. Mochizuki, H. Yokoi, H. Matsushime, K. Furuichi, Immunocyte Ca^{2+} influx system mediated by LTRPC2. *Science* **293**, 1327–1330 (2001). Medline doi:10.1126/science.1062473

41. S. Yamamoto, S. Shimizu, S. Kiyonaka, N. Takahashi, T. Wajima, Y. Hara, T. Negoro, T. Hiroi, Y. Kiuchi, T. Okada, S. Kaneko, I. Lange, A. Fleig, R. Penner, M. Nishi, H. Takeshima, Y. Mori, TRPM2-mediated Ca^{2+} influx induces chemokine production in monocytes that aggravates inflammatory neutrophil infiltration. *Nat. Med.* **14**, 738–747 (2008). Medline doi:10.1038/nm1758

42. W. P. Cheshire Jr., Thermoregulatory disorders and illness related to heat and cold stress. *Auton. Neurosci.* **196**, 91–104 (2016). Medline doi:10.1016/j.autneu.2016.01.001

43. K. Togashi, Y. Hara, T. Tominaga, T. Higashi, Y. Konishi, Y. Mori, M. Tominaga, TRPM2 activation by cyclic ADP-ribose at body temperature is involved in insulin secretion. *EMBO J.* **25**, 1804–1815 (2006). Medline doi:10.1038/sj.emboj.7601083

44. T. W. Chen, T. J. Wardill, Y. Sun, S. R. Pulver, S. L. Renninger, A. Baohan, E. R. Schreiter, R. A. Kerr, M. B. Orger, V. Jayaraman, L. L. Looger, K. Svoboda, D. S. Kim, Ultrasensitive fluorescent proteins for imaging neuronal activity. *Nature* **499**, 295–300 (2013). Medline doi:10.1038/nature12354

45. F. Tronche, C. Kellendonk, O. Kretz, P. Gass, K. Anlag, P. C. Orban, R. Bock, R. Klein, G. Schütz, Disruption of the glucocorticoid receptor gene in the nervous system results in reduced anxiety. *Nat. Genet.* **23**, 99–103 (1999). Medline doi:10.1038/12703

46. M. Lazarus, K. Yoshida, R. Coppari, C. E. Bass, T. Mochizuki, B. B. Lowell, C. B. Saper, EP3 prostaglandin receptors in the median preoptic nucleus are critical for fever responses. *Nat. Neurosci.* **10**, 1131–1133 (2007). Medline doi:10.1038/nn1949

47. C. J. Madden, S. F. Morrison, Neurons in the paraventricular nucleus of the hypothalamus inhibit sympathetic outflow to brown adipose tissue. *Am. J. Physiol. Regul. Integr. Comp. Physiol.* **296**, R831–R843 (2009). Medline doi:10.1152/ajpregu.91007.2008

48. T. E. Scammell, J. K. Elmquist, J. D. Griffin, C. B. Saper, Ventromedial preoptic prostaglandin E2 activates fever-producing autonomic pathways. *J. Neurosci.* **16**, 6246–6254 (1996). Medline

49. L. M. Harden, I. du Plessis, S. Poole, H. P. Laburn, Interleukin (IL)-6 and IL-1β act synergistically within the brain to induce sickness behavior and fever in rats. *Brain Behav. Immun.* **22**, 838–849 (2008). Medline doi:10.1016/j.bbi.2007.12.006

50. B. L. Roth, DREADDs for neuroscientists. *Neuron* **89**, 683–694 (2016). Medline doi:10.1016/j.neuron.2016.01.040

51. M. Koch, L. Varela, J. G. Kim, J. D. Kim, F. Hernández-Nuño, S. E. Simonds, C. M. Castorena, C. R. Vianna, J. K. Elmquist, Y. M. Morozov, P. Rakic, I. Bechmann, M. A. Cowley, K. Szigeti-Buck, M. O. Dietrich, X. B. Gao, S. Diano, T. L. Horvath, Hypothalamic POMC neurons promote cannabinoid-induced feeding. *Nature* **519**, 45–50 (2015). Medline doi:10.1038/nature14260

52. R. M. McAllen, M. Tanaka, Y. Ootsuka, M. J. McKinley, Multiple thermoregulatory effectors with independent central controls. *Eur. J. Appl. Physiol.* **109**, 27–33 (2010). Medline doi:10.1007/s00421-009-1295-z

53. C. J. Gordon, *Temperature Regulation in Laboratory Rodents* (Cambridge Univ. Press, 1993).

54. L. Vong, C. Ye, Z. Yang, B. Choi, S. Chua Jr., B. B. Lowell, Leptin action on GABAergic neurons prevents obesity and reduces inhibitory tone to POMC neurons. *Neuron* **71**, 142–154 (2011). Medline doi:10.1016/j.neuron.2011.05.028

55. L. Borgius, C. E. Restrepo, R. N. Leao, N. Saleh, O. Kiehn, A transgenic mouse line for molecular genetic analysis of excitatory glutamatergic neurons. *Mol. Cell. Neurosci.* **45**, 245–257 (2010). Medline doi:10.1016/j.mcn.2010.06.016

56. Y. Matsuoka, T. Furuyashiki, H. Bito, F. Ushikubi, Y. Tanaka, T. Kobayashi, S. Muro, N. Satoh, T. Kayahara, M. Higashi, A. Mizoguchi, H. Shichi, Y. Fukuda, K. Nakao, S. Narumiya, Impaired adrenocorticotropic hormone response to bacterial endotoxin in mice deficient in prostaglandin E receptor EP1 and EP3 subtypes. *Proc. Natl. Acad. Sci. U.S.A.* **100**, 4132–4137 (2003). Medline doi:10.1073/pnas.0633341100

57. J. A. Boulant, Counterpoint: Heat-induced membrane depolarization of hypothalamic neurons: An unlikely mechanism of central thermosensitivity. *Am. J. Physiol. Regul. Integr. Comp. Physiol.* **290**, R1481–R1484, discussion R1484 (2006). Medline

58. S. Kobayashi, A. Hori, K. Matsumura, H. Hosokawa, Point: Heat-induced membrane depolarization of hypothalamic neurons: A putative mechanism of central thermosensitivity. *Am. J. Physiol. Regul. Integr. Comp. Physiol.* **290**, R1479–R1480, discussion R1484 (2006). Medline doi:10.1152/ajpregu.00655.2005

59. W. Riedel, G. Maulik, Fever: An integrated response of the central nervous system to oxidative stress. *Mol. Cell. Biochem.* **196**, 125–132 (1999). Medline doi:10.1023/A:1006936111474

60. S. S. Evans, E. A. Repasky, D. T. Fisher, Fever and the thermal regulation of immunity: The immune system feels the heat. *Nat. Rev. Immunol.* **15**, 335–349 (2015). Medline doi:10.1038/nri3843

61. H. Knowles, Y. Li, A. L. Perraud, The TRPM2 ion channel, an oxidative stress and metabolic sensor regulating innate immunity and inflammation. *Immunol. Res.* **55**, 241–248 (2013). Medline doi:10.1007/s12026-012-8373-8

62. A. Di, X. P. Gao, F. Qian, T. Kawamura, J. Han, C. Hecquet, R. D. Ye, S. M. Vogel, A. B. Malik, The redox-sensitive cation channel TRPM2 modulates phagocyte ROS production and inflammation. *Nat. Immunol.* **13**, 29–34 (2012). Medline doi:10.1038/ni.2171

63. J. Eberwine, T. Bartfai, Single cell transcriptomics of hypothalamic warm sensitive neurons that control core body temperature and fever response: Signaling asymmetry and an extension of chemical neuroanatomy. *Pharmacol. Ther.* **129**, 241–259 (2011). Medline doi:10.1016/j.pharmthera.2010.09.010

64. I. Chowers, N. Conforti, S. Feldman, Local effect of cortisol in the preoptic area on temperature regulation. *Am. J. Physiol.* **214**, 538–542 (1968). Medline

65. J. L. McClellan, J. J. Klir, L. E. Morrow, M. J. Kluger, Central effects of glucocorticoid receptor antagonist RU-38486 on lipopolysaccharide and stress-induced fever. *Am. J. Physiol.* **267**, R705–R711 (1994). Medline

66. D. L. Court, S. Swaminathan, D. Yu, H. Wilson, T. Baker, M. Bubunenko, J. Sawitzke, S. K. Sharan, Mini-λ: A tractable system for chromosome and BAC engineering. *Gene* **315**, 63–69 (2003). Medline doi:10.1016/S0378-1119(03)00728-5

67. J. H. Kim, S. R. Lee, L. H. Li, H. J. Park, J. H. Park, K. Y. Lee, M. K. Kim, B. A. Shin, S. Y. Choi, High cleavage efficiency of a 2A peptide derived from porcine teschovirus-1 in human cell lines, zebrafish and mice. *PLOS ONE* **6**, e18556 (2011). Medline doi:10.1371/journal.pone.0018556

68. D. R. Shimshek, J. Kim, M. R. Hübner, D. J. Spergel, F. Buchholz, E. Casanova, A. F. Stewart, P. H. Seeburg, R. Sprengel, Codon-improved Cre recombinase (iCre) expression in the mouse. *Genesis* **32**, 19–26 (2002). Medline doi:10.1002/gene.10023

69. F. W. Farley, P. Soriano, L. S. Steffen, S. M. Dymecki, Widespread recombinase expression using FLPeR (flipper) mice. *Genesis* **28**, 106–110 (2000). Medline doi:10.1002/1526-968X(200011/12)28:3/4<106::AID-GENE30>3.0.CO;2-T

70. C. G. Lobe, K. E. Koop, W. Kreppner, H. Lomeli, M. Gertsenstein, A. Nagy, Z/AP, a double reporter for Cre-mediated recombination. *Dev. Biol.* **208**, 281–292 (1999). Medline doi:10.1006/dbio.1999.9209

71. L. Madisen, T. A. Zwingman, S. M. Sunkin, S. W. Oh, H. A. Zariwala, H. Gu, L. L. Ng, R. D. Palmiter, M. J. Hawrylycz, A. R. Jones, E. S. Lein, H. Zeng, A robust and high-throughput Cre reporting and characterization system for the whole mouse brain. *Nat. Neurosci.* **13**, 133–140 (2010). Medline doi:10.1038/nn.2467

72. A. Cetin, S. Komai, M. Eliava, P. H. Seeburg, P. Osten, Stereotaxic gene delivery in the rodent brain. *Nat. Protoc.* **1**, 3166–3173 (2006). Medline doi:10.1038/nprot.2006.450

73. J. T. Ting, T. L. Daigle, Q. Chen, G. Feng, Acute brain slice methods for adult and aging animals: Application of targeted patch clamp analysis and optogenetics. *Methods Mol. Biol.* **1183**, 221–242 (2014). Medline doi:10.1007/978-1-4939-1096-0_14

74. L. Tian, S. A. Hires, T. Mao, D. Huber, M. E. Chiappe, S. H. Chalasani, L. Petreanu, J. Akerboom, S. A. McKinney, E. R. Schreiter, C. I. Bargmann, V. Jayaraman, K. Svoboda, L. L. Looger, Imaging neural activity in worms, flies and mice with improved GCaMP calcium indicators. *Nat. Methods* **6**, 875–881 (2009). Medline doi:10.1038/nmeth.1398

75. A. H. Hopman, F. C. Ramaekers, E. J. Speel, Rapid synthesis of biotin-, digoxigenin-, trinitrophenyl-, and fluorochrome-labeled tyramides and their application for in situ hybridization using CARD amplification. *J. Histochem. Cytochem.* **46**, 771–777 (1998). Medline doi:10.1177/002215549804600611

76. A. Watakabe, N. Ichinohe, S. Ohsawa, T. Hashikawa, Y. Komatsu, K. S. Rockland, T. Yamamori, Comparative analysis of layer-specific genes in mammalian neocortex. *Cereb. Cortex* **17**, 1918–1933 (2007). Medline doi:10.1093/cercor/bhl102